NTNU
Department of Chemical Engineering

TKP4580 - CHEMICAL ENGINEERING,
SPECIALIZATION PROJECT

Modelling and estimation of a semi-batch reactor for miniemulsion polymerization of vinyl chloride monomer

Author
Jørgen Troøyen

Supervisors
Johannes Jäschke
Anne Øyen Halås

December 15, 2022

Abstract

The aim of this project was to develop a dynamic model of a miniemulsion polymerization of vinyl chloride monomer (VCM). The motivation of the project was to explore the possibilities of implementing Nonlinear Model Predictive Control (NMPC). Polymerization reactors usually have nonlinear dynamics, which means that NMPC could be a good candidate to improve operation. It is necessary for the process model to be sufficiently accurate for a successful implementation of NMPC. This report presents all necessary model equations, involving kinetics, phase equilibria and energy balances for the cooling system of the reactor. In addition, general theory of the governing mechanisms of miniemulsion polymerization are presented. The work done in this project has been completed in collaboration with Cybernetica AS and INOVYN Norge. This project has been a continuation of a summer internship at Cybernetica AS.

The process model was implemented in C-code by using Cybernetica's model template for polymerization processes. Simulations of the model was performed in Cybernetica's tool ModelFit, while necessary model inputs and measurements were provided by INOVYN. Model parameters were either adjusted manually or obtained by offline parameter estimation in order to fit the model to the provided measurements. An online state- and parameter estimation was then implemented. The model was validated by simulating three additional, arbitrary batches.

The plots obtained from the ballistic simulations gave tolerable results, but some mismatch from measurements was observed. The mismatch, especially in the reactor temperature, suggested that the implementation of online estimation was necessary. Simulations with online estimation showed great improvement and the model predictions were in good agreement with the measurements. All four simulated batches showed similar results, with only minor individual characteristics for each batch. Based on the similarity in the results from simulations of all four batches with online estimation it was concluded that the accuracy of the model was satisfactory. This further meant that the model could be used for the implementation of NMPC in further work.

Table of Contents

List of Figures

List of Tables

List of Symbols

Some comments regarding notation are listed to establish consistency:

- Superscript lower case letters are used for phases when describing mass, volume, concentration, moles, etc: Free phase (f), gas phase (g), polymer phase (p), water/aqueous phase (w).
- Subscript upper case letters are used for species when describing mass, volume, concentration, moles: Initiator (I), monomer (M), polymer (P), radical (R), surfactant/cosurfactant (S), water (W).
- Superscript lower case letters are also used when describing physical properties: Gaseous state (g), liquid state (l), solid state (s)

Latin symbols

Symbol	Description	Unit
A_J^{amb}	Cooling jacket - ambient area	m^2
A_R^{amb}	Reactor - ambient area	m^2
A_{reflux}	Reflux condenser area	m^2
A_R^J	Reactor - cooling jacket area	m^2
AX	Chain transfer agent	
a_S	Interfacial area of particles	m^2
C	Relative rate coefficient, radical termination in polymer phase	1/s
CF	Correction factor for kinetic parameters	
$C_{p,cw}^{reflux}$	Heat capacity, cooling water to condenser	J/kg/K
$C_{p,i}^{feed}$	Heat capacity, inlet specie i	J/kg/K
$C_{p,J}$	Heat capacity, water inside jacket	J/kg/K
$C_{p,reflux}$	Heat capacity, water inside condenser	J/kg/K
D_i	Dead polymer chain of length i	
d_p	Particle diameter	m
f	Initiator efficiency	
$\hat{f}_i^0$	Fugacity of specie i at standard state	Pa
$\hat{f}_i^j$	Fugacity of specie i in phase j	Pa
I	Initiator	
K_c	Intermediate calculation parameter	m^3/mol/s
K_H	VCM-in-water solubility constant	kgVCM/kgH_2O
K_k	Kalman filter gain matrix	
K_s	Correction factor for solubility of VCM in PVC	
k	Parameter in Smith & Ewart equation	
k'	Rate coefficient for radical exit	1/s
k_{abs}	Absorption rate constant	m^3/mol/s
k_{ct}^{AX}	Rate constant, chain transfer to CTA	m^3/mol/s
k_{ct}^{M}	Rate constant, chain transfer to monomer	m^3/mol/s
k_{ct}^{P}	Rate constant, chain transfer to polymer	m^3/mol/s
k_{des}	Desorption rate constant	1/s
k_i	Rate constant, chain initiation	1/s
k_i^A	Rate constant, chain initiation by CTA	1/s
k_d	Rate constant, initiator decomposition	1/s
k_p	Rate constant, propagation reaction	m^3/mol/s
k_t	Rate constant, termination	m^3/mol/s
k_{tc}	Rate constant, termination by combination	m^3/mol/s

k_{td}	Rate constant, termination by disproportionation	$m^3/mol/s$
k_t^p	Rate constant, termination in polymer phase	$m^3/mol/s$
k_t^w	Rate constnat, termination in water phase	$m^3/mol/s$
M	Monomer; Vinyl chloride	
M_i	Molar mass of specie i	kg/mol
$\hat{m}_{cw}^{reflux}$	Mass flow, cooling water to condenser	kg/s
m_i	Total mass of specie i	kg
$\hat{m}_i^{feed}$	Inlet mass flow of specie i, reactor	kg/s
m_i^j	Mass of specie i in phase j	kg
m_J	Mass of water inside cooling jacket	kg
$\hat{m}_J$	Inlet mass flow, water to jacket	kg/s
m_M^{tot}	Total mass of monomer fed	kg
m_P	Total mass of polymer	kg
m_{reflux}	Mass of water inside condenser	kg
N_A	Avogadros number	1/mol
$N_{p(n)}$	Number of particles with n radicals	
N_T	Total amount of moles of particles	mol
$\bar{n}$	Average number of radicals per particles	
n_i	Total amount of moles of specie i	mol
$\hat{n}_i$	Inlet molar flow of specie i	mol/s
$n_{i,0}$	Initial moles of specie i	mol
n_i^j	Amount of moles of specie i in phase j	mol
P	Polymer; Polyvinyl chloride	
P_i	Growing polymer chain of length i	
P_{tot}	Total amount of moles of radicals	mol
p_k	Subset of all model parameters	
p_M	Partial pressure of monomer	Pa
p_M^{sat}	Saturation pressure of monomer	Pa
p_R	Reactor pressure	Pa
p_W	Partial pressure of water	Pa
p_W^{sat}	Saturation pressure of water	Pa
R	Gas constant	J/mol/K
$R\cdot$	Radical	
R_d	Reaction rate, decomposition of initiator	$mol/m^3/s$
R_I	Reaction rate, chain initiation	$mol/m^3/s$
R_p	Reaction rate, propagation/polymerization	mol/s
R_t	Reaction rate, termination	$mol/m^3/s$
S	Surfactant	
T_{amb}	Ambient temperature	K
$T_{cw,r}^{in}$	Temperature, cooling water to condenser	K
$T_{cw,r}^{out}$	Temperature, cooling water from condenser	K
T_i^{feed}	Temperature, inlet specie i, to reactor	K
T_J	Cooling jacket temperature	K
T_J^{in}	Temperature, water to jacket	K
T_J^{out}	Temperature, water from jacket	K
T_R	Reactor temperature	K
T_{reflux}	Reflux condenser temperature	K
T^g	Gas temperature	K
U_J^{amb}	Cooling jacket-ambient heat transfer coefficient	$W/m^2/K$
U_R^{amb}	Reactor-ambient heat transfer coefficient	$W/m^2/K$
U_{reflux}	Condenser heat transfer coefficient	$W/m^2/K$
U_R^J	Reactor-cooling jacket heat transfer coefficient	$W/m^2/K$
u_k	Input vector	

$V_{fluid,s}$	Volume of liquid and solids with neither monomer or water in gas phase	m^3
V_R	Reactor volume	m^3
V^j	Volume of phase j	m^3
v_k	Process noise vector	
v^p	Volume of a polymer particle	m^3
W	Water	
w_k	Measurement noise vector	
x_k	State vector	
$[X]^j$	Concentration of specie X in phase j	mol/m^3
X_M	Monomer conversion	
X_M^{final}	Final monomer conversion	
$\hat{x}_k$	State estimate	
$\bar{x}_k$	A priori state estimate	
x_k^a	Augmented state vector	
$y_{m,k}$	Measurement vector	
y_k	Predicted model outputs vector	
y_M	Molar fraction of monomer in gas phase	
y_W	Molar fraction of water in gas phase	

Greek symbols

Symbol	Description	Unit
α_M	Monomer activity	
ΔH_{rx}	Heat of reaction	kJ/mol
ϵ	Ratio of total termination that is due to termination by disproportionation	
θ	Model parameters vector	
θ_{max}	Upper bounds on model parameters	
θ_{min}	Lower bounds on model parameters	
μ	Rate of increase in volume of particle	m^3/s
ϱ	Volumetric rate of formation of radicals	
ρ_i^j	Density of specie i in phase j	kg/m^3
σ	Average rate of radical entry to particles	$1/s$
φ	Volume fraction of polymer in polymer phase	
Φ	Parameter that varies between 0 and 2	
χ	Flory-Huggins interaction parameter	

List of Abbreviations

CMC	Critical Micelle Conscentration
CTA	Chain Transfer Agent
EKF	Extended Kalman Filter
KF	Kalman Filter
MHE	Moving Horizon Estimation
NMPC	Nonlinear Model Predictive Control
P-PVC	Paste-Polyvinyl Chloride
PVC	Polyvinyl Chloride
Redox	Reduction-oxidation
RK2	2^{nd} order Runge Kutta
S-PVC	Suspension-Polyvinyl Chloride
SQP	Sequential Quadratic Programming
VCM	Vinyl Chloride Monomer

1 Introduction

1.1 Background

Synthetic polymers in the form of plastics are an integral part of our everyday life. Plastics have a wide range of properties and applications. One of the most used plastics is polyvinyl chloride (PVC), which is a thermoplastic polymer. PVC can possess a variety of properties by the introduction of additives[1]. It has a low cost and relatively low requirement for petroleum raw materials due to its chloride content[1]. This makes PVC a much used material in various sectors. Nearly 50 million tonnes of PVC are produced world wide each year, with Norwegian-based production contributing to about 200 000 tonnes[1]. The production in Norway takes place at INOVYN's plant at Herøya Industrial Park. There are several PVC types produced at Herøya, with paste-PVC (P-PVC) being one of them. P-PVC is produced by miniemulsion polymerization of vinyl chloride monomer (VCM).

The work in this report was performed in collaboration with Cybernetica AS and INOVYN Norge. This project is a continuation of a summer internship at Cybernetica and will extend further into a master thesis. This report looks into the miniemulsion polymerization of VCM. Polymerization processes in general have nonlinear dynamics which can arise from various phenomena, such as the highly exothermic nature of the polymerization reaction and the complex kinetics[2]. Due to the nonlinearity of the process Nonlinear Model Predictive Control (NMPC) can be a good candidate to improve operation. The NMPC could for instance improve the control of the reactor temperature, which is of great importance due to the exothermic polymerization reaction. NMPC could also be utilized to reduce the required time to reach satisfactory conversion, the so called batch time. Optimization of the batch time would result in higher production capacity and profits. In order to improve operation with the implementation of NMPC, it is necessary for the process model to reflect the real process in a satisfactory manner. Thus, the motivation of this project was to develop a sufficiently accurate model so that NMPC can be successfully implemented in a later stage.

1.2 Literature

Several studies have looked into the modelling of polymerization of VCM, with the two most relevant papers presented here. The polymerization processes described in the two papers are suspension polymerization processes, which is another type of polymerization process.

Kiparissides et al.[3] developed a model of a PVC batch suspension reactor. The model predicts several key parameters, such as the monomer concentration in the gas-, aqueous and polymer phases, polymerization rate and reactor temperature. Relevant assumptions for simplifying the model are also presented. The accuracy of the developed model was demonstrated through the simulation of experimental data reported in literature. Also, an experimental reactor was deployed in order to validate the model. The results showed that the model predictions were in good agreement with the experimental results.

Mejdell et al.[4] developed a model of an industrial suspension-PVC (S-PVC) reactor, which is deployed at INOVYN's plant at Herøya Industrial Park. Compared to other models in literature, such as the one described above, this paper has its main focus on the cooling system of the reactor. A reflux condenser connected to the top of the reactor was included in the cooling system. The model for the reactor temperature and outlet temperature of the cooling jacket was compared to measured data from a test where the reactor only contained water. The modelled outlet temperature of the cooling jacket was compared with measurements taken during production. Both the water test and the test during operation showed promising results.

1.3 Scope of Work

This project aims to develop a model for the miniemulsion polymerization of VCM performed in a semi-batch reactor at INOVYN's plant. The model was implemented in C-code in one

of Cybernetica's model templates for polymerization processes and simulated in Cybernetica's tool ModelFit. Both ballistic simulations and simulations with online state- and parameter estimation was performed. Based on the simulation results, a conclusion to whether or not the model performance was satisfactory could be drawn.

This project was undertaken as part of the specialization course TKP4580 at the Department of Chemical Engineering at NTNU.

1.4 Structure of the Report

Section 2 first present general theory of polymerization. Then the theoretical aspects of both emulsion- and miniemulsion polymerization are presented, as the two processes are closely linked. Section 3 explains the software used, while section 4 includes the process description along with some general assumptions. Section 5 presents the model of the miniemulsion polymerization, including kinetics, material balances, phase equilibria and energy balances. In section 6 the simulation results are presented. This section also includes the discussion of the simulations. Finally, section 7 contains the conclusions and recommendations for further work.

Citations which are placed after a period in the last sentence in a paragraph are connected to the entire paragraph. Citations before a period at the end of sentence are connected to the particular sentence(s).

2 Theoretical Aspects

This section gives an introduction to the theory of polymers and polymerization processes. Some general topics are covered before the governing mechanisms of emulsion- and miniemulsion polymerization are presented. This includes the kinetics of free-radical polymerization and distinctive features of emulsion- and miniemulsion polymerization. In addition to theory about relevant chemistry and kinetics, state- and parameter estimation are also briefly covered.

2.1 Polymers and Polymerization

Polymers are large macromolecules built up by smaller units called monomers. The numerous ways the monomers can arrange themselves give rise to many desirable properties in polymers, spanning from elasticity to hardness and tensile strength[5]. One of the most common polymers is PVC which is comprised of VCM. The PVC polymer chain is shown in equation 2.1.

$$[-C_2H_3Cl-]_n \tag{2.1}$$

The number n represent the number of repeating monomer units, i.e. the polymer length. PVC is an example of a linear polymer, which is one of the three main groups of polymers. The two others are branched polymers and cross-linked polymers. Linear polymers are arranged in a linear sequence, while branched polymers and cross-linked polymers have a more complex structure. Branched polymers have, as the name imply, branches of varying length stretching out of the main sequence. Linear polymers can be packed densely leading to properties such as stiffness, strength and optical clarity. Branched polymers are unable to pack densely due to the presence of the branches. Cross-linked polymers are formed by linking together linear polymer chains in a process called cross-linking or vulcanization. Cross-linked polymers display elastomeric, or rubber-like properties. [5]

PVC is also an example of a homopolymer. Homopolymers are polymers comprised of only one type of monomer, excluding the ends. The formation of such polymers are called homopolymerization[6]. Another example of homopolymerization is the polymerization of propylene to polypropylene. Polymers comprised of two or more monomer species are often referred to as copolymers. An example of a copolymerization product is SB-plastic which is comprised of the two monomers styrene and butadiene[7]. Copolymers are divided further into groups depending on how the different monomer species arrange themselves. The different types of copolymers are random-, block-, periodic- and graft-polymers. Figure 2.1 shows the different types of copolymers along with a general homopolymer.

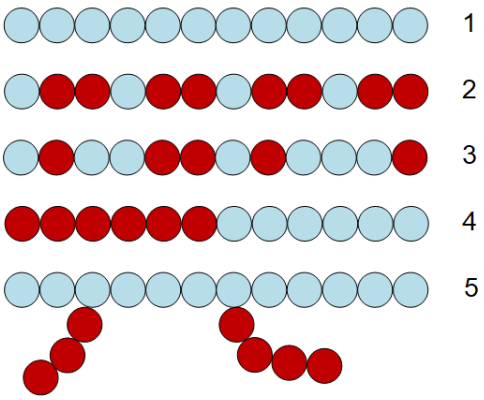

Figure 2.1: Homopolymer (1), Periodic polymer (2), Random polymer (3), Block polymer (4) and Graft polymer (5).

Polymerization reactions can mainly be divided into two types; step growth polymerization and chain growth polymerization. Step growth polymerization is also known as condensation

polymerization and is performed with monomers and polymers having reactive groups. The reactive groups may condense intermolecularly, eliminating a small by-product. This by-product is generally water[8]. A general step-growth polymerization is shown in equation 2.2.

$$\mathrm{x{-}mer} + \mathrm{y{-}mer} \longrightarrow (\mathrm{x}+\mathrm{y}){-}\mathrm{mer} \tag{2.2}$$

Here x and y represent every combination of positive integers, meaning polymer chains can react with both monomers and other polymer chains. Condensation polymers often form more slowly than addition polymers with high molecular weights only being achieved towards the end of the reaction[8].

In chain growth polymerization the reaction proceeds with the rapid addition of monomers to the active site of a growing polymer chain. The active site is then transferred to the newly added monomer[8]. The growth of the polymer chain usually lasts only for a short period of time meaning that the reaction mixture mostly consists of inactive polymer chains, growing polymer chains and unchanged monomer[8]. The polymerization of VCM to PVC is an example of a chain growth polymerization process, which usually proceeds with the following mechanisms: initiation, propagation, chain transfer and termination.

2.2 Free-Radical Polymerization

The mechanism of free-radical polymerization belongs to the class of chain growth polymerization. Polymerzation of VCM into PVC, which is modelled in this project, is an example of a free-radical polymerization process. For free-radical polymerization the active centre is free radicals. The increase in chain length is very rapid due to the reactive nature of the radicals. A free-radical polymerization start with initiation, which is then followed by propagation, chain transfer and termination. [9]

2.2.1 Reaction mechanisms for homopolymerization

Initiation

The initiation of a free-radical polymerization process consists of two parts: initiator decomposition and chain initiation. The initiator decomposition creates free radicals which then can initiate a polymer chain. The free radicals can be produced in several ways. The simplest mechanism is thermal decomposition through the homolytic cleavage of a covalent bond. One initiator molecule splits into two radicals as shown in equation 2.3 [10].

$$\mathrm{I} \xrightarrow{k_d} 2\,\mathrm{R}\cdot \tag{2.3}$$

Here I is the initiator, R· is the formed radical and k_d is the rate constant for the initiator decomposition. The decomposition rate of the initiator can then be expressed as

$$R_d = k_d[I], \tag{2.4}$$

where $[I]$ is the concentration of initiator. The radicals formed by the initiator are referred to as primary radicals. Primary radicals can react further with monomer molecules. This is referred to as chain initiation and the reaction is shown in equation 2.5.

$$\mathrm{R}\cdot + \mathrm{M} \xrightarrow{k_i} \mathrm{P}_1 \tag{2.5}$$

Here M is a monomer molecule, P_1 is a polymer radical of length one and k_i is the rate constant for the chain initiation reaction. After this reaction the active site is located at the polymer chain. Only a fraction of the primary radicals formed actually initiates a new polymer chain. This is due to various mechanisms that make the radicals inactive. Thus, an initiator efficiency,

f, is introduced. The initiator efficiency generally lies in the range of 0.4 - 0.9 [10]. This leads to the rate expression for chain initiation shown in equation 2.6.

$$R_I = 2k_d f[I] \tag{2.6}$$

The right hand side of equation 2.6 is multiplied by two because the thermal decomposition generates two radicals per initiator molecule.

Generating free radicals can also be done by reduction-oxidation (redox) systems. This is a very effective method of generating free radicals under mild conditions[11]. A great advantage of this initiation method is that the radical production is reasonable over a wide temperature range[9]. The method is widely used for initiating polymerization processes that operate at low to intermediate temperatures. At these temperatures thermal initiators either give too slow or too rapid radical generation[11]. A typical redox system is comprised of a hydroperoxide, with the chemical formula ROOH, and a reducing agent, often a metal[11]. The described mechanism is shown in equation 2.7.

$$\mathrm{ROOH} + \mathrm{Mt^k} \longrightarrow \mathrm{RO\cdot} + \mathrm{Mt^{k+1}} + \mathrm{OH^-} \tag{2.7}$$

In the above equation, $\mathrm{Mt^k}$ and $\mathrm{Mt^{k+1}}$ represent a metal in oxidation state k and $k+1$, respectively. The metal acts as a catalyst while it participates in complex formation with other species in the reaction system. If monomer is present in a system like this, the polymerization is initiated by the reaction between the alkoxy radical (RO·) and a monomer molecule[12]. An example of a peroxide-metal initiator system is a $\mathrm{H_2O_2}-\mathrm{Fe^{2+}}$ redox system, often called Fenton's reagent[11]. The polymerization of several vinyl monomers are initiated by this mechanism. Due to the complexity of the reaction mechanisms involved in a redox system, these systems are much more difficult to model compared to a thermal initiator system.

Propagation

Propagation is the successive addition of monomer molecules to the active site. Each addition creates a new radical with the same identity as the previous, except that it is one monomer molecule longer[9]. The general form of a propagation reaction is shown in equation 2.8.

$$\mathrm{P_i} + \mathrm{M} \xrightarrow{k_p} \mathrm{P_{i+1}} \tag{2.8}$$

Here k_p is the propagation rate constant, while $\mathrm{P_i}$ and $\mathrm{P_{i+1}}$ are polymer chain radicals of length i and $i+1$, respectively. The expression for the propagation rate of the general propagation reaction is

$$R_p = k_p[M]^p[P_{tot}]^p, \tag{2.9}$$

where $[M]^p$ is the concentration of monomer in the polymer phase and $[P_{tot}]^p$ is the total concentration of radicals in the polymer phase. The rate constant for propagation varies with chain length. The propagation involving very short chains might be approximately 10 times faster than for long chains[10]. The rate constant decreases quickly and obtains a constant value beyond a chain length of 5[13]. In most cases chains have lengths of $>>100$, so it is reasonable to consider the rate constant for propagation to be independent of chain length.

Termination

Termination is the reaction between two live polymer radicals. This reaction can occur in two ways: termination by combination and termination by disproportionation. When two polymer radicals terminate by combination the result is a dead polymer chain of length equal to the sum of the two reacted chains[13]. The result when two polymer chains terminate by disproportionation is two dead polymer chains with lengths equal to those of the live chains

at the moment of reaction[13]. The two modes of termination is shown in equation 2.10 and 2.11, respectively.

$$\mathrm{P_i} + \mathrm{P_j} \xrightarrow{k_{tc}} \mathrm{D_{i+j}} \tag{2.10}$$

$$\mathrm{P_i} + \mathrm{P_j} \xrightarrow{k_{td}} \mathrm{D_i} + \mathrm{D_j} \tag{2.11}$$

Here k_{tc} is the rate constant for termination by combination and k_{td} is the rate constant for termination by disproportionation, while D_i, D_j and D_{i+j} represents dead polymer chains. The sum of the two termination modes will yield the total termination rate, implying that

$$k_t = k_{tc} + k_{td}, \tag{2.12}$$

where k_t denotes the total termination rate constant[10]. The total rate expression for termination can then be expressed as

$$R_t = 2k_t[P_{tot}]^2 \tag{2.13}$$

The total termination rate constant will be a weighted sum of the two modes. The ratio between the two modes of termination will vary depending on the system. A common convention in literature is therefore to define

$$\epsilon = \frac{k_{td}}{k_{td} + k_{tc}}, \tag{2.14}$$

which then allows for writing k_{td} and k_{tc} as a fraction of the total termination rate constant, as shown in equation 2.15 [10].

$$\begin{aligned} k_{td} &= \epsilon k_t \\ k_{tc} &= (1-\epsilon)k_t \end{aligned} \tag{2.15}$$

The mode of termination does not influence the total termination rate, but it strongly influences the molecular weight of the polymer[12].

Chain transfer

In many polymerization systems the observed molecular weight is lower than the one predicted. This is due to the premature termination of a growing polymer chain. The growing radical takes a weakly bonded atom/specie from other molecules in the system[10]. This is generally a hydrogen atom. The transfer generates a dead polymer chain and a new radical that initiates a new polymer chain. There are three main chain transfer types: transfer to monomer, transfer to polymer and transfer to chain transfer agent (CTA). The mechanisms for the respective types are shown in 2.16, 2.17 and 2.18 [13].

$$\mathrm{P_i} + \mathrm{M} \xrightarrow{k_{ct}^M} \mathrm{D_i} + \mathrm{P_1} \tag{2.16}$$

$$\mathrm{P_i} + \mathrm{D_j} \xrightarrow{k_{ct}^P} \mathrm{D_i} + \mathrm{P_j} \tag{2.17}$$

$$\begin{aligned} \mathrm{P_i} + \mathrm{AX} &\xrightarrow{k_{ct}^{AX}} \mathrm{D_iX} + \mathrm{A}\cdot \\ \mathrm{A}\cdot + \mathrm{M} &\xrightarrow{k_i^A} \mathrm{P_1} \end{aligned} \tag{2.18}$$

The CTA is represented as AX, k_{ct}^M, k_{ct}^P, k_{ct}^{AX} are the rate constants for the chain transfer to monomer, polymer and CTA, respectively. The rate constant for the chain initiation by the CTA is denoted k_i^A. Chain transfer in free-radical polymerization is of great interest since the final properties of the polymer depends on the molecular weight[14]. In some cases chain transfer is used to introduce functionality at the polymer ends[12].

2.3 Dispersed-Phase Polymerization

In dispersed-phase polymerization the monomer is dispersed in a continuous phase, usually water. The viscosity of the mixture is to a large extent dependent on the dispersion medium, making the viscosity quite low even at high monomer conversions. This property makes agitation easier which facilitates easier heat removal. Using water as the dispersed medium has several advantages: water has high thermal conductivity, specific heat and heat of vaporisation. The high heat of vaporization creates a safety margin in the event of a reaction runaway. [13]

Dispersed-phase polymerization is a collective term which contains several different polymerization processes. In suspension polymerization a monomer-soluble initiator is used in a water-insoluble monomer which is dispersed in the aqueous phase by agitation. None, or very little surfactant is used meaning no emulsification takes place. The monomer is polymerized inside the droplets. If surfactant is added above its Critical Micelle Concentration (CMC) and a monomer-soluble initator is used, a microsuspension polymerization process is formed. Switching from a monomer-soluble to a water-soluble initiator creates an emulsion polymerization system. A microemulsion polymerization is formed by either increasing the surfactant concentration or decreasing the monomer concentration in an emulsion polymerization. Reducing the droplet size and adding a cosurfactant to an emulsion polymerization enables a miniemulsion polymerization to form. [13]

The dispersed-phase polymerization processes mentioned above are quite similar in that they contain many of the same species. In another way they are completely different and produces polymers with unique properties. Emulsion- and miniemulsion polymerization are the two processes of interest in this project. The two processes share several similarities.

2.4 Emulsion- and Miniemulsion Polymerization

Both emulsion- and miniemulsion polymerization are presented in further detail, as the two processes share several of the same characteristics. Basic concepts and mechanisms that lay the foundation for the model used in this project are discussed. In the 1940s William Harkins proposed a theory regarding the reaction loci of emulsion polymerization[15, 16]. This theory is often considered the starting-point of modern emulsion polymerization theory, with his terminology still used today[17]. The first demonstration of the miniemulsion mechanism was performed by Ugelstad et al.[18]. They showed that under the right conditions, nucleation of monomer droplets could account for a significant part of the polymer particles formed.

Emulsion polymerization is a process leading to colloidal particles dispersed in a continuous phase, generally water[10]. The diameter of the particles are in the range of 50-1000 nm and depends on the polymerization technique used[13]. Industrial production of emulsion- and miniemulsion polymers are mostly carried out in semi-batch reactors. This implies that the reactor is initially charged with monomer, emulsifiers and water, while initiator and other additives are post-dosed during the duration of the batch.

A typical miniemulsion includes water, monomer, surfactant, cosurfactant and the initiator system. Miniemulsions are produced by exposing the mixture to a high shear rate to break up the emulsion into small monomer droplets[19]. The surfactant is a surface-active agent with both hydrophilic and hydrophobic properties. In regular emulsion polymerization the task of the surfactant is to stabilize the large monomer droplets, generate micelles and stabilize the growing polymer particles[12]. In the case of miniemulsion polymerization the surfactant prevents coalescence of the small monomer droplets. In addition to the surfactant, a cosurfactant is used in miniemulsion polymerization. The main task of the cosurfactant is to prevent Ostwald ripening, which is monomer diffusion from small droplets to large droplets[20]. Cosurfactants need to be highly insoluble in the aqueous phase and highly soluble in the monomer to function properly.

In order to fully understand miniemulsion polymerization, an understanding of conventional emulsion polymerization is necessary. The two mechanisms are somewhat different, but the

main aspects are the same. The main difference is how the nucleation mechanism proceeds, and after the nucleation stage the mechanisms that control the particle growth are the same[19]. Both emulsion- and miniemulsion polymerization are complex processes with several phases and mechanisms involved. The number of phases ranges from three to four depending on the course of the reaction[20]. A general emulsion- or miniemulsion polymerization progresses through three intervals, as shown in figure 2.2.

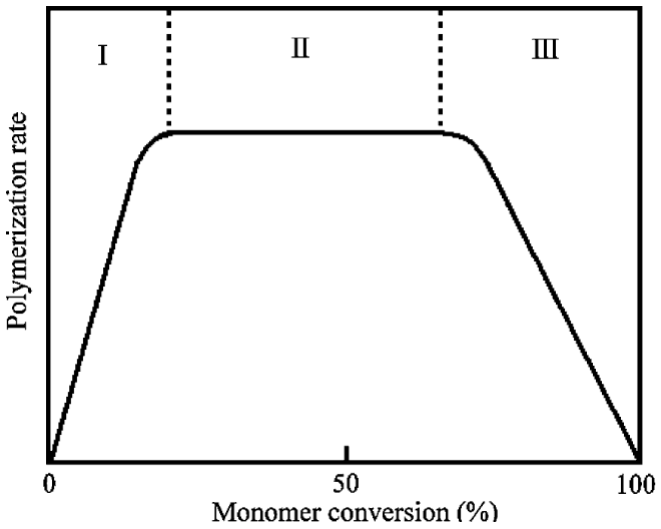

Figure 2.2: Rate of polymerization as a function of the conversion of monomer. The three intervals are labeled I, II and III.[20]

Interval I is the period where the micelles or the monomer droplets are nucleated. Interval II starts at the cessation of nucleation when the particle number becomes approximately constant. The reaction continues in interval II until there is no free monomer left. Then it enters interval III where the reaction continues without free monomer present[21].

2.4.1 Interval I - Particle Nucleation

Particle nucleation mechanisms are usually divided into three types, two of which are relevant for the distinction between emulsion- and miniemulsion polymerization. The three types of nucleation are micellar-, homogeneous- and droplet nucleation. All three mechanisms occur simultaneously, but depending on the conditions in the system one mechanism will dominate[21]. The three mechanisms has the same starting point: the initiator will decompose in the water phase and the primary radicals will react with monomer to form oligomers, which are polymer chains of few repeating monomer units[12]. The fate of the oligomers then depends on the system conditions. For homogeneous nucleation the oligomers continue to grow in the aqueous phase until they terminate or reach a critical degree of polymerization. At this point they become insoluble in water and precipitate from the water phase to form primary particles[13].

Only micellar- and droplet nucleation are covered in further detail to clarify the distinction between the dominating nucleation mechanism in emulsion- and miniemulsion polymerization.

Micellar nucleation

The primary radicals formed in the aqueous phase are hydrophilic and will keep growing in the aqueous phase until a critical chain length is reached. When a critical chain length is reached the oligomers become water-insoluble, as mentioned above. They are then able to diffuse into the micelles. The micelles then become polymer particles. The requirement for the micellar nucleation mechanism to take place is that the surfactant must be present at a concentration

above its critical micelle concentration (CMC)[13]. This means that most of the surfactant is present in the form of micelles and just some surfactant is stabilizing bigger monomer droplets. The micelles are both smaller in size and outnumbering the monomer droplets, resulting in a much greater total surface area. As a result, oligomers will have a much greater probability of being captured by a micelle than a monomer droplet, making micelle nucleation the dominant mechanism[20]. The main role of the bigger monomer droplets are to function as monomer-reservoirs for the growing particles.

Droplet nucleation

Droplet nucleation has typically been neglected in conventional emulsion polymerization. As previously mentioned all nucleation mechanisms take place, but one usually dominates. Ugelstad et al. showed how styrene monomer droplets could become stable enough to make droplet nucleation significant[18], and this became the basis for the development of miniemulsion polymerization processes.

If the monomer droplet size can be reduced to below $\sim 0.5\,\mu$m, two phenomena that enables droplet nucleation will occur. Firstly, the small droplets will be able to compete for oligomers with remaining micelles. Secondly, the reduction in droplet size will result in a huge increase in interfacial area. The new interfacial area will require surfactant to remain stable and this surfactant will be provided by the destruction of micelles. The free surfactant concentration in the aqueous phase will be well below the CMC. Not only does the small monomer droplets compete effectively with micelles, they also cause the destruction of micelles in order to keep themselves stable. This results in making droplet nucleation the dominant nucleation mechanism. A significant distinction between droplet nucleation and micellar nucleation is the nature of the particle right at the start. Where micellar nucleated particles start with low monomer concentrations, droplet nucleated particles begin as nearly 100% monomer. [21]

Interval I ends when the particle number is approximately constant. When this happens varies depending on the system, but interval I usually lasts until 2-15% conversion[9]. Once captured by either the monomer swollen micelles or the small monomer droplets the polymer chains propagate inside the generated particles.

2.4.2 Interval II - Particle Growth in the Presence of Free Monomer

As mentioned above, interval II begins at the cessation of nucleation. There are considered to be four phases present in interval II, namely gas-, aqueous-, polymer- and free phase. During interval II the particle number is considered to be constant. In addition, the particles created in interval I are considered to be the loci of the polymerization. In both emulsion- and miniemulsion polymerization interval II is considered to be when the particles grow in the presence of a free monomer phase, resulting in a constant concentration of monomer in the polymer phase[13]. In emulsion polymerization the free monomer will be located in the large monomer droplet reservoirs, while the free monomer will be inside the nucleated monomer droplets for miniemulsion polymerization. As a result the reaction mixtures will look somewhat different, as figure 2.3 shows.

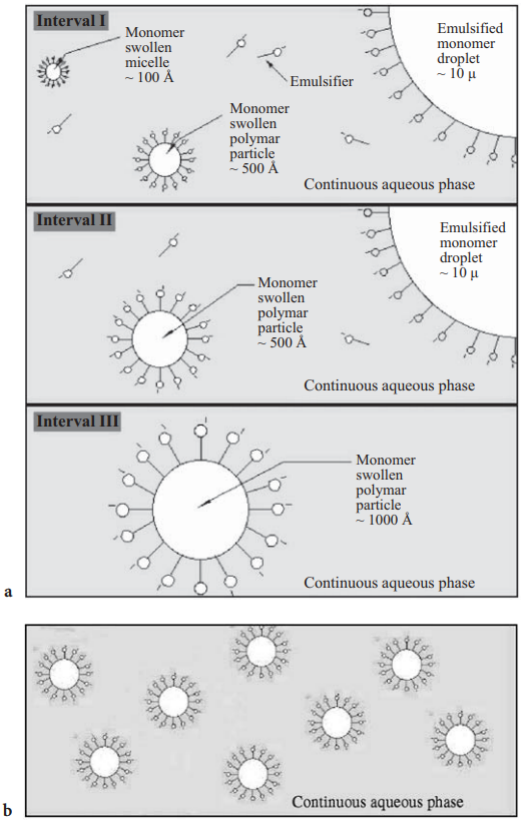

Figure 2.3: Illustration of how the reaction mixture looks like for a conventional emulsion (a) and miniemulsion (b). The figure only considers the distribution of monomer between micelles and monomer droplet, meaning other features of the reaction mixture is left out.[21]

Figure 2.3 shows that for interval II in emulsion polymerization the monomer swollen polymer particles will receive free monomer from the large emulsified monomer droplets. For miniemulsion the mechanisms happen inside the nucleated monomer droplets and the reaction mixture contains only nucleated monomer droplets. The figure only considers the distribution of monomer between micelles and droplets, and does not show oligomers, initiator and monomer dissolved in water. Interval II continues until the free monomer phase inside either the large monomer droplet reservoirs or the nucleated monomer droplets is fully consumed. At the end of interval II the number of phases drops from four to three, with the disappearance of the free monomer phase. For the polymerization of VCM the transition from interval II to interval III happens at about $70 - 80\%$[21].

2.4.3 Interval III - Particle Growth in the Absence of Free Monomer

As the free monomer phase in the system is fully consumed, the concentration of monomer in the polymer phase will no longer be constant. However, most of the monomer left will reside in the polymer phase with only some monomer present in the aqueous- and gas phase. Thus, the polymer particles will remain the loci of the reaction[13]. The reaction will continue without excess monomer present, resulting in a decrease in the monomer concentration in all three remaining phases. The concentration of monomer in all the three phases will continue to decrease until all monomer is consumed or other limiting factors stop the reaction. As the monomer inside the polymer particles is consumed the viscosity inside the particles increase, resulting in a decrease in the diffusion rate of the radicals[12]. This is the basis for the so-called autoacceleration effect.

2.4.4 Autoacceleration

One would normally expect the reaction rate of the polymerization to decrease in interval III due to the decrease in monomer concentration inside the polymer particles. This presumption can be rationalized by looking at the monomer concentration dependency of equation 2.9. However, in many polymerization processes the opposite is observed. This phenomena is often referred to as autoacceleration or the Trommsdorff-effect[9]. The effect arises from the fact that the above-mentioned termination rate in equation 2.12 is diffusion controlled. The termination rate shows a step change reduction of several orders of magnitude due to diffusion limitations caused by the increased viscosity of the reaction mixture[22]. As a result of the reduction in the termination rate, the propagation- and initiation rate are left uncontrolled. The effect is referred to as autoacceleration because the increased polymerization rate leads to a further increase in viscosity, leading to a further acceleration of the effect. Uncontrolled autoacceleration is highly undesired in industrial reactors because of the exothermic nature of most polymerization reactions. The effect can cause fast temperature rises, hot spots and erratic behavior in the reactor [22]. As a consequence, tight temperature control of the reactor is one of the most critical aspects of polymerization reactor engineering.

2.4.5 Polymerization Rate

The polymerization rate is set equal to the total propagation rate. As mentioned in section 2.2.1, the propagation rate can be written as in equation 2.9. This expression depends on the radical concentration in the polymer particles, which can vary randomly with time due to the varying particle size and the stochastic entry and exit of radicals[10]. Because of the complex nature of modelling such a system a more practical approximation is used. The approximation is based on expressing $[P_{tot}]^p$ in terms of the average number of radicals per particle. This approximation is for most practical purposes sufficiently accurate[13]. The polymerization rate can then be expressed as

$$R_p = k_p[M]^p \bar{n} N_T, \tag{2.19}$$

where $\bar{n}$ is the average number of radicals per particle and N_T is the total moles of polymer particles[10]. The product $\bar{n}N_T$ then represent the concentration of radicals in the polymer phase, $[P_{tot}]^p$. Looking at equation 2.19, it becomes evident that accurately determining the value of $\bar{n}$ and N_T is an important feature of accurately modelling a polymerization process.

2.4.6 Number of Particles

The total number of particles, N_T, is both an important and difficult parameter to predict accurately. Particle nucleation in emulsion- and miniemulsion polymerization is a complex processes that is still not well understood. Numerous investigations have been conducted in order to describe this phenomena, and Smith & Ewart were the first to propose a quantification of the number of particles in the case of micellar nucleation. The expression for the total number of particles proposed by Smith & Ewart[23] is shown in equation 2.20.

$$N_T = k \left(\frac{\varrho}{\mu} \right)^{0.4} (a_S S)^{0.6} \tag{2.20}$$

Here k is a parameter varying between 0.37 and 0.53, ϱ is the volumetric rate of formation of free radicals, μ is the rate of increase in volume of a particle, a_S is the interfacial area and S is the amount of surfactant[23]. The derivation of the expression in equation 2.20 was performed based on a styrene system, which is a monomer with low water solubility. Even though the nucleation model by Smith & Ewart describes the styrene system well, large deviations have been observed for other monomer systems[12]. Since the model fails for more water soluble monomers, alternative methods needs to be utilized. A useful technique is calculating the number of particles based on measurements of the diameter of the produced polymer particles[24]. This method is discussed in more detail in section 5.4.

2.4.7 Radical Distribution

As mentioned in section 2.4.5, $\bar{n}$ is an important parameter when modelling a polymerization process. The average number of radicals per particle is defined by

$$\bar{n} = \frac{\sum_{n=0}^{\infty} nN_{p(n)}}{\sum_{n=0}^{\infty} N_{p(n)}}, \tag{2.21}$$

where $N_{p(n)}$ is the number of particles with n radicals. The value of $N_{p(n)}$ depends on the relative rates of radical absorption, desorption and termination which are hard to model[12]. Smith & Ewart were the first to formulate an equation for $\bar{n}$ in the form of a set of population balance equations that describes $N_p(n)$. The general population balance equation for $n = 0, 1, 2, ..., j$ is shown in equation 2.22 [23].

$$\begin{aligned}\frac{dN_{p(n)}}{dt} =& \big[N_{p(n-1)} - N_p(n)\big]\sigma + \big[(n+1)N_{p(n+1)} - nN_{p(n)}\big]k' \\ &+ \big[(n+1)(n+2)N_{p(n+2)} - n(n-1)N_{p(n)}\big]C\end{aligned} \tag{2.22}$$

Here σ is the average rate of radical entry, k' is the rate coefficient for radical exit and C is the relative rate coefficient for radical termination in polymer phase[25]. There have been reported several ways of solving the general population balance, with Smith & Ewart proposing three limiting cases where the general population balance can be simplified [23].

- **Case 1,** $\bar{n} \ll 1$: The situation occurs when the rate of radical exit from a particle is much greater than the radical entry. This is the most general condition for a so-called zero-one system. In such a system, most particles will contain no radicals, some will contain one radical, and virtually none will contain more than one radical. Conventional emulsion polymerization of VCM falls into this case, with reported values of $\bar{n}$ ranging from 0.0005 to 0.1[26].
- **Case 2,** $\bar{n} = 0.5$: Radical exit is considered negligible, leaving termination and radical entry as the dominant mechanisms. This implies instantaneous termination when a second radical enters a particle already containing a radical. The average particle will contain either zero or one radical, leading to an average of 0.5. The simple nature of this case have lead to it being the most widely referenced case out of the three. El-Aaser et al. reported that miniemulsion polymerization usually falls into this case with values of $\bar{n}$ approximately equal to 0.5[27].
- **Case 3,** $\bar{n} \gg 1$: For this case the radical entry is much higher than the termination inside the particles, and termination is not instantaneous on entry of a second radical. These conditions often applies to bigger particles that allow for more than one growing polymer chain. Suspension polymerization, which is briefly described in section 2.3, often have conditions leading to case 3 [12].

Studies have shown that obtaining solutions to the general dynamic population balance in equation 2.22 are quite difficult and complex. For modelling purposes approximate procedures are utilized. Li & Brooks[25] proposed such a procedure for approximating $\bar{n}$. This procedure is discussed in further detail in section 5.5 when the modelling of the system is looked into.

2.4.8 Radical Compartmentalization

In both emulsion- and miniemulsion polymerization systems, radicals are distributed among the polymer particles. Since the particle size is so small, only an average of less than one radical is present in a particle. This leads to radical compartmentalization, which is one of the most distinctive features of emulsion- and miniemulsion polymerization. Radicals in different polymer particles cannot terminate with each other, reducing the probability of termination of free radicals. As a result, the total radical concentration is higher in emulsion- and miniemulsion

systems than for bulk systems, leading to a higher polymerization rate. Radical compartmentalization also allows for longer life-time of the radicals, resulting in polymers of higher molecular weights. Both the polymerization rate and the molecular weight can be altered by adjusting the number of particles in the system. The total concentration of radicals increases with the number of particles, while the frequency of radical entry decreases with the number of particles. A lower entry frequency allows the growing chains to grow for a longer time and achieve a higher molecular weight. On the basis of the mentioned features, both the polymerization rate and the molecular weight can be increased by increasing the number of particles. This is not possible for any other polymerization technique that is based on free-radical polymerization. [10, 19]

2.5 Polymerization Reactors

Emulsion- and miniemulsion polymers are used in a wide variety of applications, each requiring its own properties. The properties of the polymer is mostly decided inside the reactor. This means that the reactor used for polymerization should be able to control the factors that decide the properties of the polymers. Using the correct reactor type is crucial to get high quality polymers. There are mainly three types of reactors used for polymerization processes, namely batch, semi-batch and continuous reactors. Figure 2.4 shows a simplified sketch of the three reactor types.

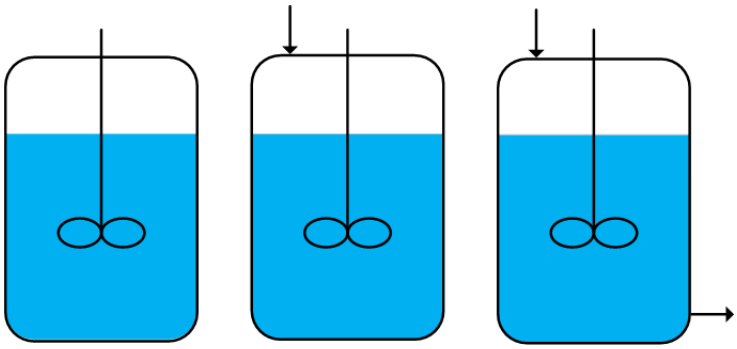

Figure 2.4: From left to right: Batch reactor, Semi-batch reactor with post-dosage, Continuous reactor.

In a batch reactor system, all reactants and additives will be charged into the reactor before the polymerization starts. Nothing is removed or added during the batch time. The major disadvantage of the batch reactor is the need for periodic shut down and start up, which is associated with a loss in polymerization time. Batch reactors are mostly used in lab-scale systems, but batch operation still finds wide use in industry. [10]

The semi-continuous stirred-tank reactor is the most widely used reactor system for polymerization processes. In a semi-continuous process a fraction of the reaction mixture is charged into the reactor before the polymerization. During the polymerization some reactants can be post-dosed, which allows for flexibility in terms of control of the reactor. Varying the amount and composition of the initial charge along with the feed rate of post-dosed reactants, both temperature and polymer properties can be controlled. For emulsion polymerization reactors, such as the one in focus in this project, it is normal to post-dose initiator. [10]

For continuous stirred-tank reactors the reactants are continuously fed to the reactor, and the products and unconsumed reactants are taken out. The reactors are operated for a long period of time without down time, and the process is often operated at steady state. Since the reactors operate continuously for extended periods, fouling can occur. Fouling is the deposition of latex on the reactor walls. The fouling will decrease the heat transfer capabilities of the reactor. In order to combat this problem the reactor has to be periodically cleaned. [10]

Due to the exothermic polymerization reaction, reactors are prone to suffer from thermal runaway. Any disturbances that changes the propagation rate will also affect the heat released by the reaction. Bearing this in mind, it is clear that the cooling system of the reactor have to be designed in such a way that it is able to handle a significant increase in the heat of reaction. If the cooling system is unable to remove sufficient heat, thermal runaway will occur[10]. Heat removal is not a problem for small scale reactors, but for high-volume reactors it becomes more challenging. This is because the large volumes make mixing harder and the temperature control slower. The risk of thermal runaway is lower in emulsion polymerization processes due the low viscosity of the reaction mixture, the high heat capacity of the water and the high heat of vaporization of the water[13]. Nevertheless, tight and robust temperature control is necessary for safe operation of a polymerization reactor.

2.6 Parameter Estimation

Models based on first principles will often contain unknown or uncertain parameters. The values for these parameters might not be obtained from literature due to the lack of available experiments performed on the relevant system. One can use parameter values from similar systems, but the values may not be exactly correct. This is the case in this work. The model used is originally a model for suspension polymerization. Estimation of some model parameters are necessary in order to make the model better reflect the real system.

2.6.1 Offline Parameter Estimation

The goal of offline parameter estimation is to estimate parameter values such that the difference between the model outputs and measurements is minimized. Cybernetica's tool ModelFit uses a Sequential Quadratic Programming (SQP) algorithm. A SQP algorithm is able to handle nonlinear model equations by iteratively solving a quadratic programming subproblem[28]. Polymerization processes are nonlinear and a SQP algorithm is necessary for the parameter estimation. The formulation of the optimization problem is shown in equation 2.23.

$$\min_{\theta} \sum_{k=1}^{N} \left(y_k - y_{m,k}\right)^2 \tag{2.23a}$$

$$\text{s.t. } x_{k+1} = f(x_k, u_k, \theta) \tag{2.23b}$$

$$y_k = g(x_k, u_k, \theta) \tag{2.23c}$$

$$\theta_{min} \leq \theta \leq \theta_{max} \tag{2.23d}$$

Here y_k is a vector containing model outputs, $y_{m,k}$ is a vector containing measurements and x_k is a vector containing the model states. θ is the decision variables for the optimization problem and is a vector containing the parameters to be estimated within the bounds θ_{min} and θ_{max}. $f(x_k, u_k, \theta)$ and $g(x_k, u_k, \theta)$ are the state- and measurement models, respectively. The SQP algorithm will minimize the objective in equation 2.23a while still fulfilling the constraints in equations 2.23b, 2.23c and 2.23d.

2.6.2 Online State- and Parameter Estimation

Models based on first principles, such as the model derived in this project, requires real time estimation of process states and uncertain process parameters. Two types of estimators used in industry are Moving Horizon Estimator (MHE) and Kalman Filter (KF), where the latter is discussed in further detail. The basic KF algorithm is derived for linear systems, but the theory can be extended to nonlinear systems by linearizing the nonlinear system at each time step[29]. This is called the Extended Kalman Filter (EKF).

The process model is assumed to be formulated on the time-discrete form

$$x_k = f(x_{k-1}, \theta, u_{k-1}, v_{k-1}) \tag{2.24}$$

$$y_k = g(x_{k-1}, \theta, u_{k-1}) + w_k, \tag{2.25}$$

where x_k represents the vector of states at time t_k, θ is the vector of parameters, u_{k-1} is the vector of inputs to the process at time t_{k-1}, v_{k-1} is the vector of process noise at time t_{k-1}, y_k is the vector of process outputs at time t_k and w_k is the vector of measurement noise at time t_k. $f(x_{k-1}, \theta, u_{k-1}, v_{k-1})$ and $g(x_{k-1}, \theta, u_{k-1})$ are the nonlinear process- and measurement-model, respectively. The EKF algorithm consists of two parts, namely a model prediction part and a measurement correction part. The model prediction part can be formulated as in equation 2.26 and 2.27.

$$\bar{x}_k = f(\hat{x}_{k-1}, \theta, u_{k-1}, \bar{v}_{k-1}) \tag{2.26}$$

$$\bar{y}_k = g(\bar{x}_{k-1}, \theta, u_{k-1}) + \bar{w}_k \tag{2.27}$$

Here $\bar{x}_k$ is the a priori state estimate, $\bar{y}_k$ is the a priori predicted measurement, $\bar{v}_{k-1}$ is the mean process noise and $\bar{w}_k$ is the mean measurement noise. The state estimate, $\hat{x}_k$, can then be calculated in the measurement correction part by equation 2.28.

$$\hat{x}_k = \bar{x}_k + K_k(y_k - \bar{y}_k), \tag{2.28}$$

Here y_k is the measurement vector and K_k is the Kalman filter gain matrix. Calculation of the Kalman filter gain matrix is based on the process noise covariance, the measurement noise covariance, the a priori state covariance and the partial derivatives of f and g, which are defined in equation 2.24 and 2.25. [30]

In order to include estimation of model parameters, an augmented state vector is used. The state vector is augmented with a parameter vector as shown in equation 2.29 [29].

$$x_k^a = \begin{pmatrix} x_k \\ p_k \end{pmatrix} \tag{2.29}$$

Here x_k^a is the augmented state vector and p_k is the vector containing the parameters that are to be estimated online. The vector p_k is a subset of all the process parameters, θ. Noise is added to the parameters through the noise parameter $v_{p,k}$ such that

$$p_k = p_{k-1} + v_{p,k-1}. \tag{2.30}$$

The process model can then be written as

$$x_k^a = f(x_{k-1}^a, \theta, u_{k-1}, v_{k-1}, v_{p,k-1}) \tag{2.31}$$

and the augmented state vector x_k^a can be estimated using the same principles as described above. Estimating parameters online will give parameter profiles. Parameter profiles have the advantage of reflecting change in parameters with time, for example the change in kinetic parameters in a polymerization process.

3 Software

This section presents the software used to implement and simulate the model, which includes Cybernetica's model template and the ModelFit environment.

3.1 Model Template

To be able to simulate the system, the model equations were implemented in C-code by using Cybernetica's model template for polymerization processes. The code for the template is confidential, meaning it is not presented in this report. States, inputs, outputs, constraints, parameters and constants, as well as internal calculation variables are all defined by the model in order to simulate the system. To solve the set of equations several integrators are readily available, namely Euler, second order Runge-Kutta (RK2) and Sundials CVODE. For this project, Euler integration was used as the integrator.

The model template facilitates easy changes to the model in the development stage. It also separates the reactor model and the kinetic model. The two models are implemented separate of each other, allowing for flexibility in terms of using the two models independently of each other. For example, different kinetic models can be tested with the same reactor design, and vice versa. Figure 3.1 shows how the model template relates to the other parts of the model development phase.

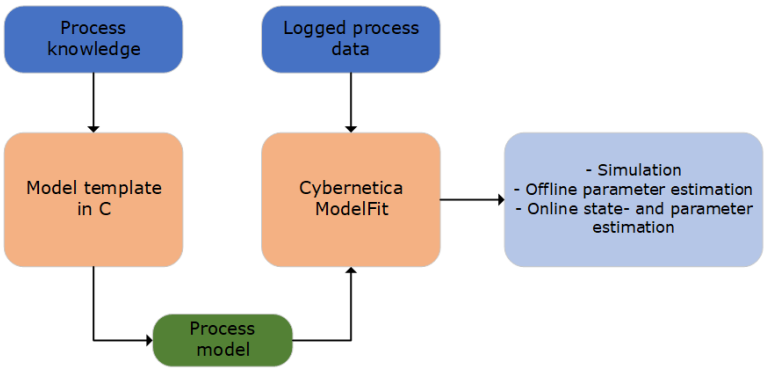

Figure 3.1: The connection between the different phases of the model development. Process knowledge is used to develop and implement a model in C. The coded process model can then be simulated in ModelFit and compared to logged process data. Both offline- and online estimation can be performed inside the ModelFit environment.

3.2 ModelFit

After the model is implemented in C-code, the model can be simulated in Cybernetica's simulation tool ModelFit. ModelFit allows for easy plotting of the simulation results, as well as flexibility when it comes to what results to display. In addition to visualizing the results, values for parameters, constants, inputs, measurements, initial conditions and noise can all be adjusted inside the ModelFit environment. The program also gives the opportunity to simulate several datasets with different model parameters simultaneously. This feature makes it simple to assess the influence a parameter has on the model.

ModelFit can also be used for offline parameter estimation, as described in section 2.6.1. Which parameter to estimate and which measurements that should be active for the estimation can both be selected inside ModelFit. The obtained parameter values can easily be implemented to the model. The parameter estimation can be done on individual datasets or on several data sets simultaneously. If the parameter estimation is done on several datasets, the parameter values obtained will be the ones that minimize the error in equation 2.23a for all the data sets.

In addition, ModelFit can also be used for online state- and parameter estimation. Then

ModelFit sees the measurements and inputs as if they were online, and not preloaded inside ModelFit as is the case for offline parameter estimation. The available estimators are MHE and EKF, with EKF used in this project as described in section 2.6.2.

As mentioned above, ModelFit offers great flexibility when it comes to visualizing the simulation results. However, for presenting simulation results in a report like this some data processing is necessary. Simulation data are therefore readily available to export from ModelFit to an appropriate file format, such as a *.mat*-file for further processing in Matlab.

4 Process Description and Assumptions

This section describes the process which is modelled. The recipe of the process along with information about some species involved are confidential and are not presented in this report. Instead, generic names are used to describe the process when needed.

The process is a miniemulsion polymerization which follows a free-radical chain polymerization mechanism as described in section 2.2 and 2.4. The initiator used is a peroxide, ROOH. Other species are also present in the reaction mixture, but are either confidential or not considered to be relevant for the modelling of the process. These species are collected under the generic name *Additive*.

4.1 Preparation of a Batch

The reactor is first charged with a pre-prepared mixture containing water, surfactant, cosurfactant and an additive that is part of the initiator system. As mentioned above, the specific names of the species are confidential and generic terms are used instead. After the pre-prepared mixture is loaded into the reactor, additional water is fed to the reactor. At this point the huge amount of droplets which the monomer will diffuse into are already formed. VCM is then added to the reactor and diffuses into the already formed droplets. The reaction mixture now consists of the monomer droplets which will act as the reaction loci for the polymerization reaction described in section 2.4. Figure 4.1 shows a typical nucleated monomer droplet with stabilizers during the polymerization reaction.

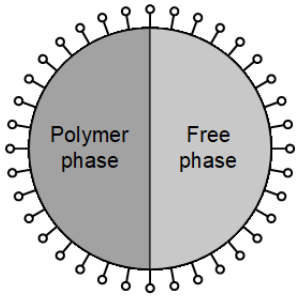

Figure 4.1: A nucleated monomer droplet with the free phase and the polymer phase each occupying some portion of the particle. The spikes on the outside of the particle are the surfactant and cosurfactant which stabilizes the particle.

When some conditions inside the reactor are met, the first dosage of initiator is fed to the reactor. However, the polymerization reaction does not start until an additive, which is also a part of the initiator system, is added to the reaction mixture.

4.2 Initiator System

The initiator mechanism is a redox-reaction as described in equation 2.7. The additive which starts the polymerization reaction leads to complex formation with the metal-ions present and the complex acts as a catalyst for the radical formation. During the course of the batch, initiator will be post-dosed.

A redox initiator mechanism is very complex, especially compared to a thermal initiator mechanism. This is due to the presence of several other components other than the initiator itself. The formation rate of primary radicals will depend on the concentration of all components that participate in the reaction mechanism and not only the initiator concentration. To be able to model the formation of primary radicals, the initiator system is approximated as a thermal initiator system as described in equation 2.3.

4.3 Reactor System

The reactor is a continuously stirred semi-batch reactor. A simplified sketch of the reactor is shown in figure 4.2. After the reaction is initialized by the dosing of the additive described in section 4.2, other additives and some water are post-dosed along with the above-mentioned initiator. Nothing is taken out from the reactor before the end of the batch.

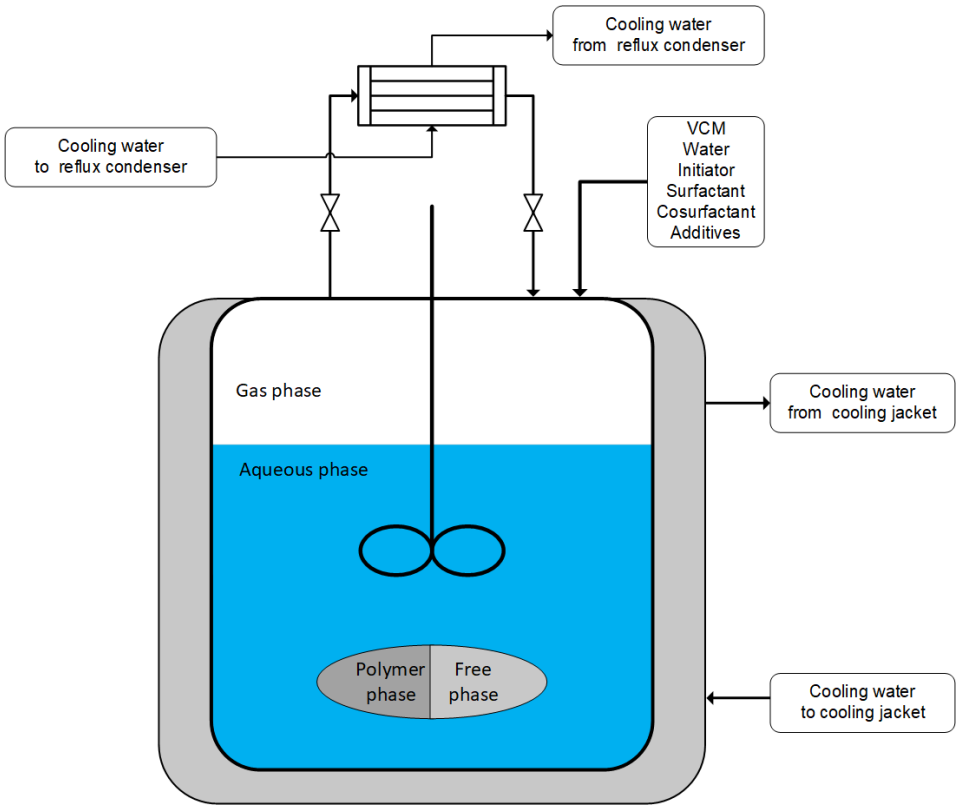

Figure 4.2: Sketch of the reactor, including the four phases present, the cooling jacket with cooling water, the reflux condenser with cooling water and the shut-off valves. In reality there are several inlet streams, but it is shown as one on the sketch for simplicity.

As can be seen from the figure, the reaction unit is comprised of three or four phases, depending on the system conditions described in section 2.4.1 - 2.4.3. The ellipse surrounding the polymer phase and free phase are just for illustration purposes and not a real depiction of what the reaction mixture looks like. Figure 4.1 better illustrates how both the free phase and the polymer phase each occupy some portion of the particles during the course of the batch.

A cooling jacket is surrounding the reactor in order to control the temperature inside the reactor. This is necessary due to the exothermic nature of the polymerization reaction as mentioned on several occasions earlier. The cooling water system related to the cooling jacket is a closed loop system to avoid fouling and corrosion inside the cooling jacket. To accompany the cooling jacket, a reflux condenser is installed in connection with the top of the reactor. The condenser provides even more cooling capabilities to the cooling system. At some point during the batch the reflux condenser is shut off using the two valves. The conditions for when the reflux condenser is closed off is further discussed in section 5.6.1.

As seen from figure 4.2 and the description of the process, several components will be present in each of the four (three) phases. In order to structure the presence of components in all phases as well as establishing notation, table 4.1 is constructed. The table shows which components that are assumed to be in which phases along with the notation involved.

Table 4.1: Overview over notation and which components are present in each phase during the course of the batch.

	Monomer	Polymer	Water	Surfactant & Cosurfactant	Initiator	Radicals
Gas phase	n_M^g	-	n_W^g	-	-	-
Aqueous/water phase	n_M^w	-	n_W^w	n_S^w	n_I^w	n_R^w
Free phase	n_M^f	-	-	-	-	-
Polymer phase	n_M^p	m_P	-	-	-	$\bar{n}N_T$
Total	n_M	m_P	n_W	n_S	n_I	$n_R^w + \bar{n}N_T$

As can be seen in table 4.1 the surfactant and cosurfactant are grouped together. This is done for modelling purposes and they are then considered to be one specie, with the collective name $Surfactant$ for simplicity. The notation in the table considers the amount of moles of each specie and in total, except for polymer. Polymer is considered on mass basis due to the varying molecular weight. Thus, it is more practical to use mass based notation.

4.4 Assumptions

The theory presented in section 2 lays the foundation of the modelling of the reactor system. Along with the background theory, several assumptions have been made in order to develop a model of the system. Some general assumptions are listed below, while additional assumptions are presented in section 5 where it is necessary.

- The initiator is assumed to be described as a thermal initiator, and the initiator is assumed to decompose in the water phase.
- Monomer- and polymer droplets are assumed to be monodisperse.
- The reaction mixture is assumed to be ideal.
- The reactor is assumed to be a lumped system with no spatial variations.
- Coalescence of particles is neglected.
- All droplets formed before VCM is added are assumed to be nucleated.
- The number of particles is assumed to be constant during the entirety of the batch.
- Nucleation occurs through droplet nucleation, and micellar and homogeneous nucleation are neglected. However, due to the pre-prepared mixture that is first charged into the reactor the number of particles is considered to be constant through the whole batch. This implies that the nucleation stage (Interval I) is not present and the system can be considered as a seeded system.
- The only reaction contributing to heat of reaction is the propagation reaction in equation 2.19.
- Additives are approximated as water with respect to physical properties and the material balances.

5 Modelling of the Reactor System

This section provides the necessary equations to model the system. Expressions and values for physical properties used in the model equations are listed in appendix A.

5.1 Kinetics

The kinetics related to the polymerization process are arguably the most complex mechanisms to model. A model of the kinetics can be done in almost as fine detail as possible. However, such a detailed model will not be of any practical use in terms of modelling. The model should balance accuracy and complexity.

5.1.1 Initiator System

As described in section 4.2 the initiator system is based on a redox reaction. This is a complicated system to model, leading to the simplification of modelling the initiator as a thermal initiator. Both the decomposition rate of the initiator and the rate of chain initiation are needed for the model and are shown in equation 5.1 and 5.2, respectively.

$$R_d = k_d[I]^w \tag{5.1}$$

$$R_I = 2k_d f[I]^w \tag{5.2}$$

Here $[I]^w$ is the concentration of initiator in the water phase, while all the other parameters are described in section 2.2.1.

5.1.2 Polymerization Rate

The polymerization rate, which is considered to be equal to the propagation rate, is expressed in equation 2.19. In order to use this expression the propagation of polymer chains in the water phase is neglected[26]. The propagation rate constant, k_p, is considered to be independent of chain length in accordance with literature presented in section 2.2.1. Equation 2.19 shows that the polymerization rate has a dependency of both $\bar{n}$ and N_T. The calculation of these two parameters is described in section 5.5 and 5.4, respectively.

5.1.3 Termination and Chain Transfer

Both termination in the polymer phase and in the water phase are considered for the model. The termination reactions affects the number of radicals per particle and the amount of radicals in the water phase. As mentioned in section 2.2.1 the termination in the polymer phase can occur through two mechanisms, namely termination by combination and termination by disproportionation. The ratio ϵ was defined in equation 2.14 and describes the portion of the termination which occur through disproportionation. For the polymerization system in this project, polymerization of vinyl chloride, termination by disproportionation is the most dominant mode[31]. Based on this ϵ is set equal to one, which gives

$$\begin{aligned} k_{td} &= k_t^p \\ k_{tc} &= 0 \end{aligned} \tag{5.3}$$

In addition to termination in the polymer phase (k_t^p) and in the water phase (k_t^w), desorption (k_{des}) and absorption (k_{abs}) of radicals also affect $\bar{n}$ and n_R^w. This is presented in further detail in section 5.5 along with the radical distribution.

Chain transfer is used to alter the properties of the produced polymer by altering the chain length. There are three types of chain transfer as described in section 2.2.1, but for the

polymerization of VCM the most significant mode is chain transfer to monomer[26]. Even though chain transfer do occur, it is not considered in the model in this project.

5.1.4 Correction Factor for Kinetic Parameters

The numeric values for the kinetic parameters used are mainly unknown or taken from models of other VCM polymerization processes. This implies that the values are uncertain. In order to alter the entire kinetic model with a single parameter, a correction factor CF is introduced to all the kinetic rate constants. The implementation of the correction factor is shown in equation 5.4.

$$\begin{aligned} k_d &= CF \cdot k'_d \\ k_p &= CF \cdot k'_p \\ k_t^p &= CF \cdot k_t^{p'} \\ k_t^w &= CF \cdot k_t^{w'} \\ k_{des} &= CF \cdot k'_{des} \\ k_{abs} &= CF \cdot k'_{abs} \end{aligned} \tag{5.4}$$

Here the dashed rate constants represent the numerical values before the multiplication with the correction factor, while the non-dashed parameters represent the values which are used for calculations in the model.

5.2 Material Balances

Material balances are necessary to describe the rate of change of each specie. The material balances are written on a molar basis except for polymer which is written on a mass basis. A generic material balance for a semi-batch reactor can be written as

$$\frac{dn_i}{dt} = \hat{n}_i + R_i, \qquad n_i(0) = n_{i,0}, \tag{5.5}$$

where the left side represents the molar rate of change of specie i, $\hat{n}_i$ represents the molar inflow of specie i, R_i is the generation/consumption of specie i and $n_{i,0}$ is the initial amount of specie i [32]. Equation 5.5 is used as the basis for the total material balances of monomer, water, surfactant and initiator. The resulting molar balances are shown in equation 5.6 - 5.9.

$$\frac{dn_M}{dt} = \hat{n}_M - R_p, \qquad n_M(0) = n_{M,0} \tag{5.6}$$

$$\frac{dn_I}{dt} = \hat{n}_I - R_d V^w, \qquad n_I(0) = n_{I,0} \tag{5.7}$$

$$\frac{dn_W}{dt} = \hat{n}_W, \qquad n_W(0) = n_{W,0} \tag{5.8}$$

$$\frac{dn_S}{dt} = \hat{n}_S, \qquad n_S(0) = n_{S,0} \tag{5.9}$$

Since the water and surfactant do not participate in any reactions, the material balances for the two species do not contain any generation/consumption terms. As mentioned briefly at the start of this section the material balance for polymer is expressed on a mass basis. This is due to the varying molecular weight of the polymer particles. Equation 5.10 shows the resulting mass based material balance for the polymer.

$$m_P(t) = X_M(t) M_M \int_0^t \hat{n}_M \, dt \tag{5.10}$$

Here M_M is the molar mass of monomer and $X_M(t)$ is the time dependent conversion of monomer, which can be expressed by equation 5.11 [32].

$$X_M(t) = \frac{\int_0^t \hat{n}_M \, dt - n_M(t)}{\int_0^t \hat{n}_M \, dt} \tag{5.11}$$

Equation 5.6 - 5.10 gives the total material balances for their respective species, but the model also requires a description of how monomer, water and radicals distribute between the phases. These calculations are presented in sections 5.3 and 5.5, respectively.

5.3 Monomer Distribution and Phase Equilibria Calculations

The monomer distributes it self in the four (three) phases during the polymerization. Calculations of the monomer distribution are based on the Flory-Huggins equation, as well as models of S-PVC reactors developed by Kiparissides et al.[3] and Mejdell et al.[4]. Based on the calculations of the monomer distribution, a sufficient description of the system can be obtained. This includes the reactor pressure, volumes of the phases and also how the other species distribute in all the phases in accordance with table 4.1. Some additional assumptions related to these calculations are listed below:

- During the polymerization the model assumes equilibrium at all times between all phases.
- The solubility of monomer in the polymer phase follows Flory-Huggins equation.
- The solubility of monomer in water phase follows Henry's law.
- The vapour phase follows the ideal gas law.
- The polymer is insoluble in the monomer.
- The gas phase is assumed to only contain monomer- and water vapor. Some residual air might be present in the gas, but the amount is assumed to be negligible.
- Volume additivity is assumed to be valid.

From the assumption of equilibrium between all phases it follows that the fugacity of the monomer in all four phases must be equal. This relation is expressed in equation 5.12.

$$\hat{f}_M^m = \hat{f}_M^p = \hat{f}_M^w = \hat{f}_M^g \tag{5.12}$$

Here $\hat{f}_M^i$ represents the fugacity of the monomer in phase i.

Depending on which interval the reaction takes place, the Flory-Huggins equation is either used to calculate the monomer activity α_M, or the volume fraction of polymer in the polymer phase, φ. The general form of the Flory-Huggins equation used in all three intervals is shown in equation 5.13.

$$\ln(\alpha_M) = \ln(1-\varphi) + \varphi + \chi\varphi^2 \tag{5.13}$$

Here χ is the temperature dependent Flory-Huggins interaction parameter and the activity of the monomer is defined as

$$\alpha_M = \frac{\hat{f}_M^p}{\hat{f}_M^0}, \tag{5.14}$$

where $\hat{f}_M^0$ is the fugacity of pure monomer at reactor temperature and saturation pressure. [3, 4]

Interval I and II

One of the assumptions made in section 4.4 stated that the system is modelled as a seeded system because of the pre-made reaction mixture. This implies that interval I is not considered. Interval I and II are then merged together when modelling the system.

When a separate monomer phase exist, i.e. the free monomer phase is present, the monomer activity will be equal to one, yielding equation 5.15 [3].

$$\ln(1) = 0 = \ln(1-\varphi) + \varphi + \chi\varphi^2 \tag{5.15}$$

From equation 5.15 the volume fraction of polymer in the polymer phase can be calculated. This is done iteratively since an analytical solution cannot be obtained. The calculation also includes the expression for the interaction parameter χ. The code used for solving equation 5.15 is shown in appendix C.4 and C.7, while the code performing the rest of the calculations for interval I and II is shown in appendix C.3. The obtained volume fraction can be used to calculate the mass of monomer in the polymer phase from equation 5.16.

$$m_M^p = K_s \left(\frac{\rho_M^l m_p}{\rho_P} \right) \left(\frac{1-\varphi}{\varphi} \right) \tag{5.16}$$

Here ρ_P and ρ_M^l are the density of polymer and liquid monomer, respectively. K_s is a correction factor for the solubility of the monomer in the polymer phase and it is purely a modelling parameter. The derivation of equation 5.16 is shown in appendix C.1.

Equation 5.17 shows the expression for the mass of monomer in the gas phase.

$$m_M^g = (V_R - V_{fluid,s}) \frac{\rho_M^l \rho_M^g}{\rho_M^l - \rho_M^g} \tag{5.17}$$

Here V_R is the reactor volume, ρ_M^g is the gas density of the monomer and $V_{fluid,s}$ is defined as

$$V_{fluid,s} = \frac{m_W}{\rho_W^l} + \frac{m_M}{\rho_M^l} + \frac{m_P}{\rho_P}, \tag{5.18}$$

and represents the volume of the liquid and solids in the system if neither monomer or water were present in the gas phase. m_W and m_M are the total mass of water and monomer in the system. The derivation of equation 5.17 is shown in appendix C.2.

The mass of monomer dissolved in the water phase is calculated from Henry's law and is shown in equation 5.19.

$$m_M^w = K_H \alpha_M m_W \tag{5.19}$$

The constant K_H is the VCM-in-water solubility constant and its value is equal to 0.0088 $\frac{\text{kgVCM}}{\text{kgH}_2\text{O}}$ [33]. Conservation of mass can be utilized to obtain the mass of monomer in the free phase.

$$m_M^f = m_M - m_M^p - m_M^g - m_M^w \tag{5.20}$$

Equation 5.20, along with equation 5.16, 5.17 and 5.19 fully describes the distribution of the monomer between all phases in interval I and II.

The total pressure inside the reactor will be the sum of the partial pressures of monomer and water. For interval I and II the partial pressures will be equal to their respective saturation pressures evaluated at the reactor temperature. The molar fractions in the gas for the two

species are dependent on the total reactor pressure and the saturation pressures of the two species. The relations described are shown in equation 5.21, 5.22 and 5.23, respectively[3].

$$p_R = p_M + p_W = p_M^{sat} + p_W^{sat} \tag{5.21}$$

$$y_M = 1 - y_W \tag{5.22}$$

$$y_W = \frac{p_W^{sat}}{p_R} \tag{5.23}$$

Here p_M and p_W are the partial pressures of monomer and water, while p_M^{sat} and p_W^{sat} are their respective saturation pressures. The saturation pressures are functions of temperature, both listed in appendix A. For interval I and II the gas temperature will be the same as the temperature of the liquid. The temperature of the liquid is obtained from an energy balance over the reactor.

The volumes of the four phases present are also necessary to describe the system. The calculation of the volume of the gas phase, the polymer phase, the free phase, the water phase and the liquid phase are listed in equation 5.24 - 5.28.

$$V^g = \frac{m_M^g}{y_m \rho_M^g} \tag{5.24}$$

$$V^p = \frac{m_P}{\rho_P} + \frac{m_M^p}{\rho_M^l} \tag{5.25}$$

$$V^f = \frac{m_M^f}{\rho_M^l} \tag{5.26}$$

$$V^w = V^l - V^p - V^f \tag{5.27}$$

$$V^l = V_R - V^g \tag{5.28}$$

The concentration of monomer in the polymer phase can be obtained through equation 5.29.

$$[M]^p = \frac{m_M^p}{M_M V^p} \tag{5.29}$$

Finally, the mass of water in the gas phase can be described by equation 5.30.

$$m_W^g = \frac{y_W p_R V^g M_W}{R T^g} \tag{5.30}$$

Here R is the gas constant and M_W is the molar mass of water. The equations mentioned are sufficient in describing the the physical conditions inside the reactor when excess monomer is present. When the excess monomer is fully consumed ($m_M^f = 0$) and the system enters interval III, some adjustments in the description are necessary.

Interval III

For interval III the activity of the monomer is no longer equal to one, thus the Flory-Huggins equation cannot be used to calculate φ. The volume fraction of polymer in the polymer phase is instead obtained by solving equation 5.16 with respect to φ. Then α_M is calculated by inversely solving equation 5.13. The calculations are done iteratively based on an initial guess that assumes all monomer is in the polymer phase. The calculation procedure for interval III is summarized in algorithm 1, while the necessary code is shown in appendix C.5 and C.6.

Since the activity of monomer is no longer equal to one, the partial pressure of monomer is no longer equal to the saturation pressure. The total pressure is still equal to the sum of the partial pressures of monomer and water. Equation 5.31 and 5.32 shows the two relations.

$$p_M = \alpha_M p_M^{sat} \tag{5.31}$$

$$p_R = \alpha_M p_M^{sat} + p_W^{sat} \tag{5.32}$$

The gas temperature in interval III is no longer set equal to the liquid temperature. Instead, the gas temperature is set equal to the saturation temperature of the monomer at the given partial pressure of the monomer given in equation 5.31. The necessary code to perform this calculation is shown in appendix C.8. Apart from the deviating calculations mentioned, all other calculations are performed in the same manner as for interval I and II, with $m_M^f = 0$.

Algorithm 1: Calculation procedure for interval III

Set initial guess of monomer in the polymer phase equal to the total amount of monomer in the system
for $i = 0, 1, 2, 3$ **do**
  Compute φ from eq. 5.16
  Compute α_M from eq. 5.13
  Compute reactor pressure from eq. 5.32
  Compute gas temperature from partial pressure of monomer given in eq. 5.31
  Compute mass of monomer in gas phase and water phase as in interval I and II
  Compute mass of monomer in polymer phase from conservation of mass from eq. 5.20 with $m_M^f = 0$
  Update initial guess as the weighted sum of previous value and the new calculated value of monomer in the polymer phase
end
Proceed with the same calculations as in interval I and II.

5.4 Number of Particles

As mentioned in section 2.4.6, predicting the number of particles is difficult. Smith & Ewart's theory presented in equation 2.20 shows large deviations for polymerization of VCM[34]. This implies that another method must be utilized.

The model assumes that the number of particles is constant during the whole batch. This allows for a backwards calculation of the number of particles based on measurements of a previous batch. From this the amount of particles can be expressed as

$$N_T = \frac{m_p^{tot}}{m_p^{particle} N_A} = \frac{m_M^{tot} X_M^{final}}{v^p \rho_P N_A}, \tag{5.33}$$

where m_M^{tot} is the total mass of monomer fed to the reactor from a previous batch, X_M^{final} is the final conversion from a previous batch, ρ_P is the density of the polymer particle, N_A is Avogadro's number and v^p is the volume of a polymer particle. The volume of a polymer particle can be written as

$$v^p = \frac{\pi}{6} d_p^3 \tag{5.34}$$

Here d_p is the diameter of the polymer particle and is found from analysis of the produced polymer from a previous batch. The number of particles will then be constant from batch to batch, independent of disturbances. This might lead to some inaccuracies in the model. However, according to INOVYN the pre-made mixture described in section 4.1 is repeatable. As a result of this the number of particles will be quite stable from batch to batch, meaning that the approximation in equation 5.33 is relatively accurate.

5.5 Radical Distribution

The radical distribution is modelled using an approximation of $\bar{n}$ proposed by Li & Brooks[25]. The proposed approximation yields a simple differential equation describing $\bar{n}$ and is shown in equation 5.35.

$$\frac{d\bar{n}}{dt} = \sigma - k_{des}\bar{n} - \Phi C\bar{n}^2 \tag{5.35}$$

Here σ is the average rate at which radicals enter the particles, k_{des} is the rate coefficient for radical exit from the particles, C is the relative rate coefficient for radical termination in the polymer phase and Φ is a coefficient which ranges from 0 to 2 [25]. Expressions for σ, Φ and C are shown in equations 5.36, 5.37 and 5.38, respectively.

$$\sigma = \frac{k_{abs}n_R^w}{V^w} \tag{5.36}$$

$$\Phi = \frac{2(2\sigma + k_{des})}{2\sigma + k_{des} + C} \tag{5.37}$$

$$C = \frac{k_t^p N_T}{V^p} \tag{5.38}$$

In the above equations k_{abs} is the absorption rate constant, n_R^w is the amount of radicals in the water phase and k_t^p is the termination rate constant in the polymer phase. The amount of radicals in the water phase will change during the batch so it is necessary to be able to describe this change. The differential equation describing the change in the amount of radicals in the water phase can be expressed as

$$\frac{dn_R^w}{dt} = R_I V^w + k_{des}\bar{n}N_T - k_t^w \frac{{n_R^w}^2}{V^w} - \frac{k_{abs}n_R^w}{V^w}N_T, \tag{5.39}$$

where k_t^w is the termination rate in the water phase[10]. Equation 5.35 and 5.39 will govern the radical distribution in the system.

5.6 Energy Balances

The presented energy balances are adapted from the general energy balance given by Fogler[32] and are derived in appendix B.

5.6.1 Reactor Temperature

To achieve tight control of the reactor temperature, a sufficiently good model is necessary. The energy balance describing the change in reactor temperature is shown in equation 5.40.

$$\frac{dT_R}{dt} = \frac{Q_R^{amb} + Q_R^J + Q_{feed} + Q_{rx} + Q_{reflux}}{\sum m_i C_{p,i} + m_{steel}C_{p,steel}} \tag{5.40}$$

Here Q_R^{amb} is the heat loss to the environment, Q_R^J is the heat exchange with the cooling jacket, Q_{feed} is the energy change due to post-dosing of species, Q_{rx} is the heat of reaction, Q_{reflux} is the heat exchange with the reflux condenser, $\sum m_i C_{p,i}$ is the heat capacity of the mixture and $m_{steel}C_{p,steel}$ is the heat capacity of the reactor steel. The terms in the numerator in equation 5.40 are defined as follows:

$$Q_R^{amb} = U_R^{amb}A_R^{amb}(T_{amb} - T_R) \tag{5.41}$$

$$Q_R^J = U_R^J A_R^J (T_J - T_R) \tag{5.42}$$

$$Q_{feed} = \sum \hat{m}_i^{feed} C_{p,i}^{feed} (T_i^{feed} - T_R) \tag{5.43}$$

$$Q_{rx} = (-\Delta H_{rx}) R_p \tag{5.44}$$

$$Q_{reflux} = \begin{cases} \hat{m}_{cw}^{reflux} C_{p,CW}^{reflux} (T_{cw,r}^{in} - T_{cw,r}^{out}), & \text{when } \textit{Condition 1} \\ 0, & \text{when } \textit{Condition 2} \end{cases} \tag{5.45}$$

In the above equations U_i^j is the relevant overall heat transfer coefficient, A_i^j is the relevant heat transfer area, T_{amb} is the ambient temperature, $\hat{m}_i^{feed}$ is the inflow of specie i, $C_{p,i}^{feed}$ is the heat capacity of inlet specie i, T_i^{feed} is the temperature of inlet specie i, ΔH_{rx} is the heat of reaction, $\hat{m}_{cw}^{reflux}$ is the flow of cooling water to the reflux condenser, $C_{p,CW}^{reflux}$ is the heat capacity of the cooling water, while $T_{cw,r}^{in}$ and $T_{cw,r}^{out}$ are the inlet- and outlet temperature of the cooling water for the condenser. The cooling jacket temperature T_J is defined as

$$T_J = \frac{T_J^{in} + T_J^{out}}{2}, \tag{5.46}$$

and is the average of the inlet- and outlet temperature of the water to the cooling jacket. *Condition 1* and *Condition 2* in equation 5.45 determines when the reflux condenser is shut off using the valves depicted in figure 4.2. The exact details of these conditions are confidential.

5.6.2 Cooling Jacket Outlet Temperature

The change in the outlet temperature of the cooling jacket can be written as

$$\frac{dT_J^{out}}{dt} = \frac{Q_J^{amb} - Q_R^J + Q_{flow}}{m_J C_{p,J}}, \tag{5.47}$$

where Q_J^{amb} is the heat loss from the cooling jacket to the environment, Q_R^J is as defined in equation 5.42, Q_{flow} is the energy change from the flow of cooling water and $m_J C_{p,J}$ is the heat capacity of the water inside the cooling jacket. Q_J^{amb} and Q_{flow} are defined as

$$Q_J^{amb} = U_J^{amb} A_J^{amb} (T_{amb} - T_J) \tag{5.48}$$

$$Q_{flow} = \hat{m}_J C_{p,J} (T_J^{in} - T_J^{out}), \tag{5.49}$$

where $\hat{m}_J$ is the water flow to the cooling jacket and T_J^{in} is the temperature of the inlet water.

5.6.3 Reflux Condenser Outlet Temperature

The change in temperature of the cooling water out of the reflux condenser is shown in equation 5.50.

$$\frac{dT_{reflux}^{out}}{dt} = \frac{Q_{reflux} + Q_{ex}}{m_{reflux} C_{p,reflux}} \tag{5.50}$$

Here $m_{reflux} C_{p,reflux}$ is the heat capacity of the water inside the reflux condenser, Q_{reflux} is as defined in equation 5.45 and Q_{ex} is defined as follows:

$$Q_{ex} = U_{reflux} A_{reflux} (T^g - T_{reflux}) \tag{5.51}$$

In equation 5.51 T^g is the gas temperature in the reactor and T_{reflux} is defined as the average between the inlet- and outlet temperature of the cooling water as shown in equation 5.52.

$$T_{reflux} = \frac{T_{cw,r}^{in} + T_{cw,r}^{out}}{2} \tag{5.52}$$

6 Results and Discussion

This section presents and discusses the simulation results. The section is divided into four subsections which covers four main topics.

6.1 Offline Parameter Estimation

This section presents the obtained values for model parameters, as well as discussing issues related to the parameter estimation. The final parameter values used in the model are listed in table 6.1. Uncertain model parameters were obtained by either manual adjustment or by offline parameter estimation using ModelFit. Kinetic parameters for the initiator, as well as parameters related to the number of particles and the reactor design are not listed in table 6.1. This is because this information is confidential. Kinetic parameters for the propagation rate constant and the termination rate constant were taken from a model of S-PVC.

Table 6.1: Final parameter values used in the model. Values for the propagation rate constant, termination rate constant and the intermediate calculation parameter, K_c, was obtained from literature[3]. Kinetic parameters for the initiator, parameters related to the number of particles and the reactor design are not listed due to confidentiality.

Parameter	Value	Unit
k_p	$5 \cdot 10^5 \exp(-3320/T_R)$	$m^3/mol/s$
K_c	$1.01 \cdot 10^{-7} \exp(-5740(1/T_R - 1/333.15))$	$m^3/mol/s$
k_t^p	$2k_p^2/K_c$	$m^3/mol/s$
k_{ads}	0.2	$m^3/mol/s$
k_{des}	10^{-5}	1/s
k_t^w	0.9	$m^3/mol/s$
U_R^J	320	$W/m^2/K$
U_{reflux}	330	$W/m^2/K$
f	0.7	-
K_s	1.2	-
CF	3.6	-

The efficiency factor, f, was for simplicity set to a fixed value of 0.7 in accordance with the literature presented in section 2.2.1. The parameters k_{abs}, k_{des} and k_t^w were all unknown parameters which affect the radical distribution. To obtain values for these parameters, they were systematically altered to produce a reasonable profile for the average number of radicals per particle. The decomposition rate constant for the initiator, k_d, was adjusted to obtain a reasonable profile for the mass of initiator in the reactor. As both $\bar{n}$ and the mass of initiator in the reactor are unmeasurable, there are some uncertainty related to the obtained parameter values. Temperature dependence in the form of an Arrhenius-type expression was tested on k_{abs}, k_{des}, k_t^w and k_d. This did not result in better model performance and only introduced more unknown parameters to the model.

Both of the overall heat transfer coefficients, U_R^J and U_{reflux}, were obtained through estimation in ModelFit followed by minor manual adjustments to get a better fit in relevant regions. The overall heat transfer coefficient between the cooling jacket and the reactor was obtained by minimizing the difference in measured and modelled outlet temperature of the cooling jacket. The temperature difference between the inlet- and outlet temperature of the cooling jacket is quite small. This is most likely due to a large flow of water through the cooling jacket, resulting in a small volumetric heat transfer. As a consequence of this the outlet temperature will be insensitive to the heat transfer coefficient U_R^J to a certain extent. The outlet temperature will rather be more dependent on the inlet temperature of the water. Even though the outlet temperature of the cooling jacket is insensitive to U_R^J, the reactor temperature is reliant on an accurate value. A too low value for the coefficient can lead to thermal runaway due to

the exothermic nature of the polymerization reaction. If the coefficient was set too high the reactor temperature would decrease until it reached the jacket temperature. Thus, the reactor temperature had to be considered as well in addition to the outlet temperature of the cooling jacket when obtaining a value for U_R^J. The obtained value of $320\,\mathrm{W/m^2/K}$ gave acceptable results for both temperatures.

For the overall heat transfer coefficient for the reflux condenser, the difference in measured and modelled outlet temperature of the cooling water was minimized. Figure 6.7 shows that an adequate fit was achieved with the obtained value of $330\,\mathrm{W/m^2/K}$. The modelled temperature does not quite follow the measured temperature. A possible reason for this is that the heat transfer coefficient varies throughout the batch due to viscosity changes in the condensed monomer. The constant value does not reflect these changes.

There are two parameters which are purely modelling parameters, namely K_s and CF. These parameters were adjusted manually to give a better fit with measurements. The correction factor for the kinetic parameters was difficult to obtain, as it affects the entire kinetic model. It was first estimated in ModelFit, but this did not give a realistic result even though the result was optimal in a purely mathematical sense. The parameter was then adjusted manually to give a good fit for model outputs, especially the reactor temperature and the monomer conversion. A value of 3.6 gave acceptable results in the model outputs. The correction for the solubility of monomer in the polymer phase was altered to mainly adjust when the free monomer phase disappeared, but also partly to get a better prediction of the reactor pressure. This implied that some mismatch in the pressure had to be tolerated to more accurately predict the disappearance of the free monomer phase. A value of K_s equal to 1.2 gave the best combined result for the disappearance of the free monomer phase and the reactor pressure.

The parameter values obtained through manual fitting or estimation in ModelFit formed the basis of the simulations presented in section 6.2 and 6.4.

6.2 Ballistic Simulations

The parameter values listed in table 6.1 were implemented in four different batches. Only the results from one batch are shown in this section, but in section 6.4 the estimated parameter values for all four batches are shown to validate the model. As mentioned in section 3 the model template allows for separation of the reactor model and the kinetic model. This separation facilitates the use of measured reactor temperature in the kinetic model. For the ballistic simulations this was done to make the kinetic model independent of any errors in the reactor model. To prevent presenting confidential information, the time is shown as relative time. Most of the model outputs are plotted as functions of conversion as this is considered most relevant.

Figure 6.1 shows the evolution of the conversion through the batch. It can be seen that the polymerization reaction starts at about 20% time and goes towards 100% conversion at the end of the batch. From 0-20% time the reactor model is charged with water, monomer, surfactant and additives as described in section 4.1.

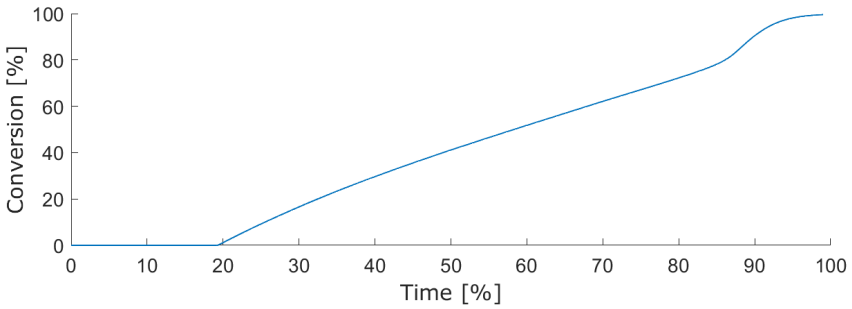

Figure 6.1: Modelled monomer conversion as a function of time. The simulation was run without recursive filtering.

Figure 6.2 shows the profiles of the average number of radicals per particle and mass of initiator in the reactor. The average number of radicals per particles immediately jumps up to 0.5 and remains constant throughout the batch. The value of 0.5 coincides with the literature presented in section 2.4.7. The constant value of $\bar{n}$ throughout the batch is a result of the parameter values from table 6.1 which was used in the Li & Brooks approximation. Some accumulation of initiator in the reactor can be seen before the mass of initiator goes towards zero at the end of the batch.

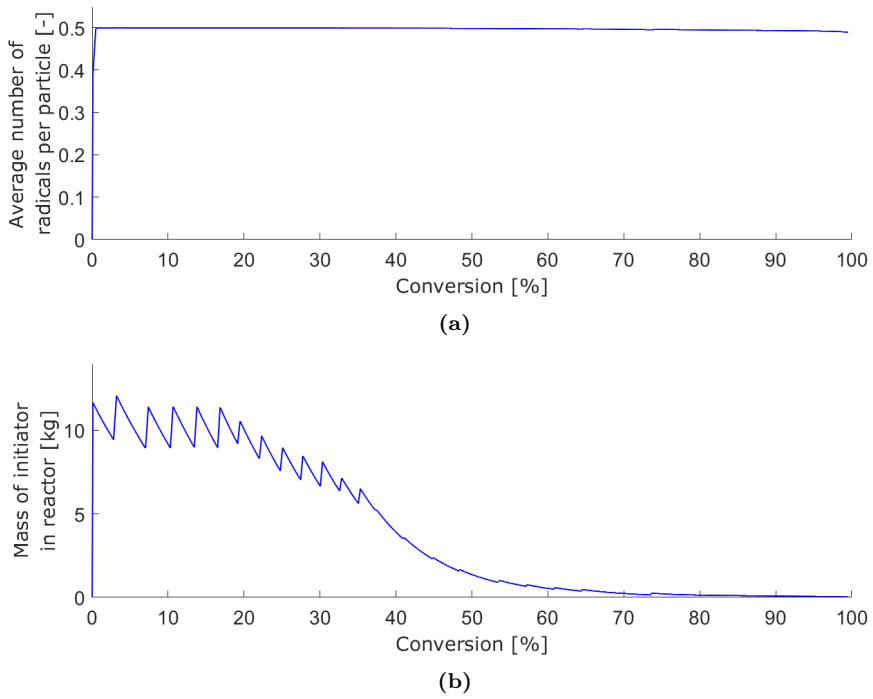

Figure 6.2: Average number of radicals per particle **(a)** and mass of initiator in reactor **(b)**. The simulation was run without recursive filtering.

The observed spikes in the mass of initiator in the reactor are due to post-dosing of initiator. As mentioned in section 6.1 there is uncertainty related to the kinetic parameters which govern the radical distribution and decomposition of the initiator. This is due to the fact that the profiles shown in figure 6.2 cannot be measured, and other untested output profiles could have given better results. The profiles are though considered to be reasonable based on knowledge from INOVYN and that other model outputs have an acceptable agreement with measurements.

Figure 6.3 shows how the modelled reactor temperature coincides with the measured reactor temperature. It also shows the gas temperature. The gas temperature is equal to the measured temperature before the cessation of free monomer, and after it deviates from the liquid temperature. The reason it is equal to the measured temperature and not the modelled temperature is because the measured temperature was used as the input to the kinetic- and phase equilibria calculations. Modelled reactor temperature follows the same trends as the measured reactor temperature, but some mismatch is observed throughout the batch. The mismatch is significantly largest at the end of the batch where the modelled temperature increases much less steeply than the measured temperature.

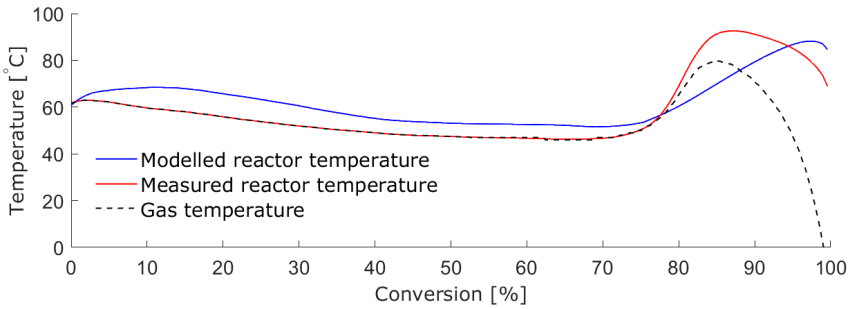

Figure 6.3: Modelled and measured reactor temperature, in addtion to the gas temperature. The simulation was run without recursive filtering.

A possible reason for the large deviation towards the end of the batch is that the model for $\bar{n}$ does not consider the Trommsdorff-effect. As mentioned in section 2.4.4 this effect results in a decrease in the termination rate, which in turn will lead to a rise in the number of radicals per particle. The average number of radicals in figure 6.2a would increase towards the end of the batch if the model considered the Trommsdorff-effect. An increase in $\bar{n}$ would lead to an increase in the reaction rate. Increasing the reaction rate would result in more heat released and a greater temperature rise. With the Trommsdorff-effect considered the modelled reactor temperature would maybe have a steeper increase and follow the measured temperature better towards the end of the batch.

Figure 6.4 shows that the modelled reactor pressure fits well with the measured pressure up to about 76% conversion. At this point the model predicts a pressure increases, while the measured pressure decreases.

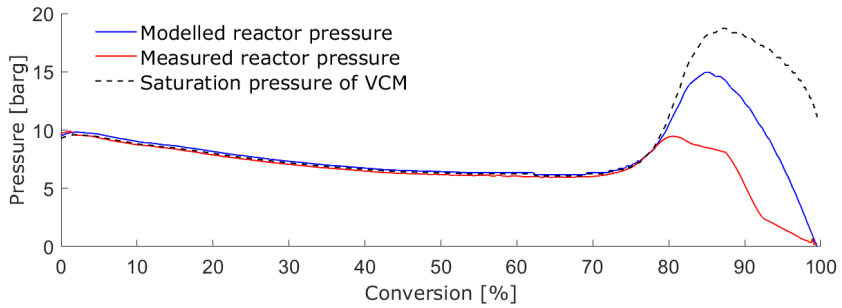

Figure 6.4: Modelled and measured reactor pressure, in addition to the saturation pressure of monomer. The simulation was run without recursive filtering.

The deviation is most likely due to the modelled pressure being mainly dependent on temperature in the form of the saturation pressures. The saturation pressures are functions of temperature as seen in appendix A. With the temperature increase in figure 6.3 the saturation

pressures will also increase. The reason that the modelled pressure is lower than the saturation pressure of monomer after about 76% conversion is because the partial pressure of monomer is multiplied with the monomer activity which is less than one after the disappearance of the free monomer phase. This is shown in equation 5.31. Due to the poor prediction of the reactor pressure towards the end of the batch, there are reasons to believe that the gas temperature in figure 6.3 also deviates from reality. This is because the gas temperature in interval III is closely connected to the reactor pressure, as described in section 5.3. Since there is no measurement of the gas temperature, this cannot be confirmed.

Figure 6.5 shows how the monomer distributes itself in the four phases throughout the batch. Most of the monomer is located in the free phase with a growing fraction located in the polymer phase. Only tiny amounts of monomer are present in the gas and water phases through the entirety of the batch.

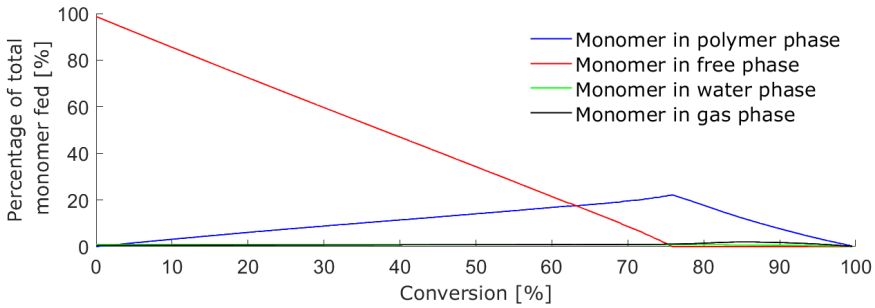

Figure 6.5: The distribution of monomer in all four phases. The simulation was run without recursive filtering.

From figure 6.5 the point where the free phase disappears is determined to be 76%. This coincides well with literature, which states that the cessation of the free monomer phase is in the range 70 - 80% [21]. The good match with literature is a result of fine tuning the monomer distribution at the expense of the accuracy in the reactor pressure. The fine tuning was done by adjusting K_s. The modelled pressure is also dependent on this parameter, meaning that some of the mismatch in the reactor pressure towards the end probably is due to the good fit in figure 6.5.

Figure 6.6 shows the modelled and measured outlet temperature of the cooling jacket, along with the measured inlet temperature. Only small deviations between the modelled temperature and measured temperature can be observed, with significant deviations only between 80% and 90%. In this part the modelled temperature has the same trend, but the change is not as large as in the measured temperature. It is worth noting the small temperature difference between the inlet and outlet. As mentioned in section 6.1 the small temperature difference will make the modelled temperature insensitive to the overall heat transfer coefficient to a certain extent. As a result of this the modelled temperature will resemble the measured temperature quite well independent of the parameter value.

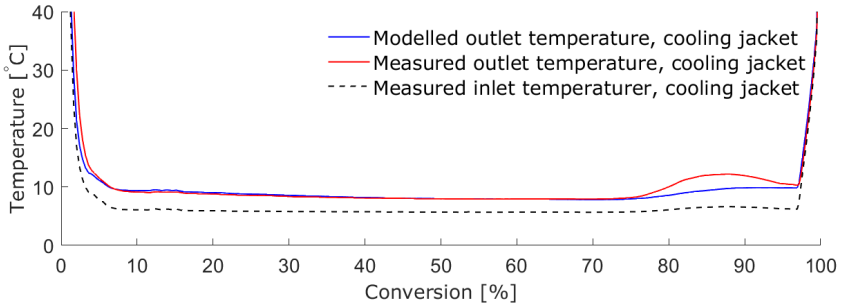

Figure 6.6: Modelled and measured outlet temperature of the cooling jacket, in addition to measured inlet temperature of the cooling jacket. The simulation was run without recursive filtering.

Figure 6.7 shows the modelled and measured outlet temperature for the reflux condenser. The modelled temperature follows the same trend as the measured temperature, but it is not able to follow the more rapid variations.

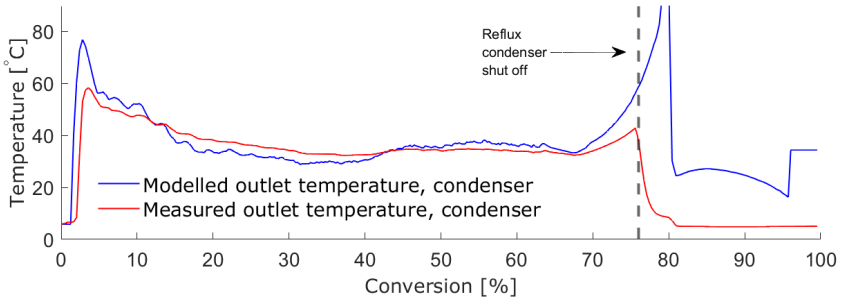

Figure 6.7: Modelled and measured outlet temperature of the reflux condenser. The simulation was run without recursive filtering.

At about 76% conversion the reflux condenser is shut off. From this point the modelled temperature have a large mismatch with the measured temperature, but this is irrelevant since the reflux condenser is disconnected from the reactor. The modelled temperature follows the measured temperature in an acceptable manner in the regions of interest.

6.3 The Model

The results presented in section 6.2 show that the ballistic simulations did not give good enough accuracy compared to the plant measurements. The mismatch could be due to various reasons, with some of them already discussed. In addition, the mismatch could arise from other sources related to the model itself. One of which could be the simplified initiator mechanism. As mentioned in section 4.2 the initiator mechanism is actually a redox mechanism, but the model assumes a thermal initiator mechanism. The simplification can be one of the reasons for the constant mismatch observed in the reactor temperature in figure 6.3. This is because the simplification might not capture the complex dynamics of the redox mechanism.

Another reason for the mismatch might be the simplified calculation of the number of particles. The number of particles is assumed to be constant from the start of the batch and this simplifies the modelling. A downside to simplifying the modelling of the number of particles is that the nucleation stage is not considered. The number of particles might be too large at the very start of the batch, resulting in a higher reaction rate at the start. The higher reaction rate will lead to a larger heat of reaction, making the reactor temperature higher. A solution to

this could be to make the number of particles start from zero and reach the final number at a given, relatively small conversion. The number of particle will then behave like a ramp at the start of the batch before reaching its constant value.

Two important assumptions made was the assumptions of an ideal mixture and that there is equilibrium between all phases at all times. These two assumptions are most likely not fulfilled some of the time, especially towards the end of the batch. The two assumptions make the system dynamics faster, as the reactions might be limited by mass transfer in reality. As an example, the initiator which is post-dosed need some time to diffuse into the reaction mixture in order to decompose and react. A solution to this could be to introduce a time constant to model the delay when dosing the initiator, for instance.

The deviations from the measurements could also be caused by the lack of viscosity dependency in the model. During the course of the batch the viscosity changes. The viscosity change affects the behavior of the system with regards to both kinetics and heat transfer. In the simulations above, parameters such as the overall heat transfer coefficients and the correction factor for kinetic parameters are constant throughout the batch. As a consequence the parameters do not capture the changes in the physical conditions in the reactor. A possible way of capturing the condition changes during the batch is to model the parameters as a function of conversion, e.g. $CF(X_M)$. A function giving the parameters from the conversion could be fitted in order to yield a better prediction of model outputs, which is of great interest.

6.4 Simulations with Recursive Filtering

The mismatch between measurements and the model outputs, especially in the reactor temperature, motivated the implementation of recursive filtering. The recursive filtering was implemented tuning the KF, which is one of the available estimators for recursive filtering mentioned in section 3. With the recursive filtering active the modelled reactor temperature was used in the kinetic- and phase equilibria calculations.

A natural choice was to estimate the correction factor for the kinetic parameters. This is because the kinetic model used was adapted from a model of a S-PVC process. Also, the mechanisms taking place in a miniemulsion polymerization are complex and the model will most likely fail to capture all aspects of it. Online estimation of CF will capture the change in conditions and correct for model errors throughout the batch. As mentioned in section 6.3 the model does not consider viscosity dependency. This suggested that choosing to estimate the two heat transfer coefficients, U_R^J and U_{reflux}, was favourable. Online estimation of U_R^J and U_{reflux} could better capture the effect of viscosity changes and fouling throughout the batch. For the recursive filtering the reactor temperature, the outlet temperature of the cooling jacket and the outlet temperature of the reflux condenser was chosen as the active measurements.

Figure 6.8 shows that the conversion with recursive filtering behaves quite similarly to the conversion from the ballistic simulations. However, it is worth noting that the conversion with recursive filtering has a steeper increase towards the end of the batch. This steeper increase means that the conversion goes faster towards 100%. The good prediction of the reactor temperature in figure 6.10 might suggest that the conversion profile obtained with recursive filtering closer reflects reality. In the simulation with recursive filtering the reaction "is finished" at an earlier batch time. This is the reason the simulation with recursive filtering does not propagate as far in time as the ballistic simulation. Plots of the model outputs will look slightly different compared to the plots in section 6.2 due to the slight difference between the conversion profiles in figure 6.8. The plotted measurement values are identical in the two cases which means that the plots from the two sections are comparable regarding mismatch with measurements.

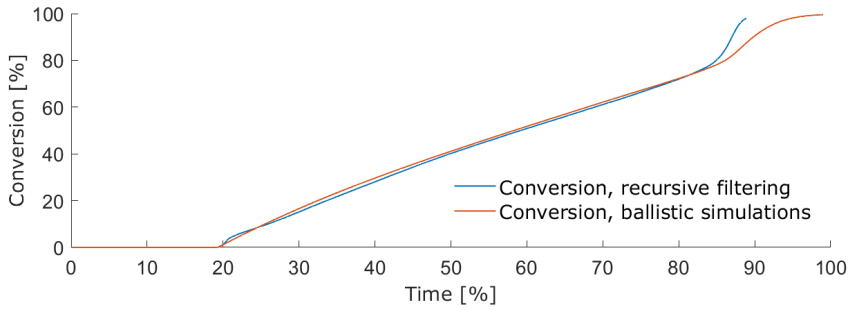

Figure 6.8: Modelled monomer conversion as a function of time. The simulation was run with recursive filtering.

Both the average number of radicals and mass of initiator in the reactor in figure 6.9 does not change significantly compared to the ballistic simulations. The minor changes are mainly due to the changes in CF during the batch. The profiles obtained are still considered to be reasonable on the same basis as in section 6.2.

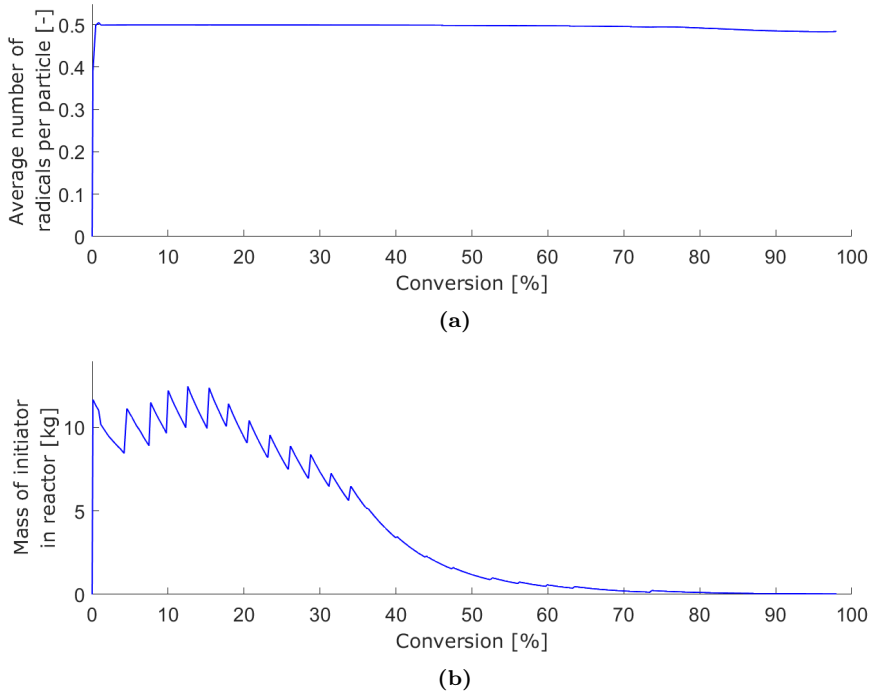

Figure 6.9: Average number of radicals per particle **(a)** and mass of initiator in the reactor **(b)**. The simulation was run with recursive filtering.

Figure 6.10 shows the modelled and measured reactor temperature, as well as the gas temperature. Significant improvement can be observed with the recursive filtering. The modelled temperature accurately reflects the measured temperature with only a slight mismatch at the end of the batch. One possible explanation to this slight mismatch can be that the estimator could not quite keep up with the drastic temperature rise. The temperature rise is not as prominent when the temperature is plotted as a function of conversion. Figure D.1 in the appendix shows the temperature plotted as a function of time which better highlights the steep temperature increase.

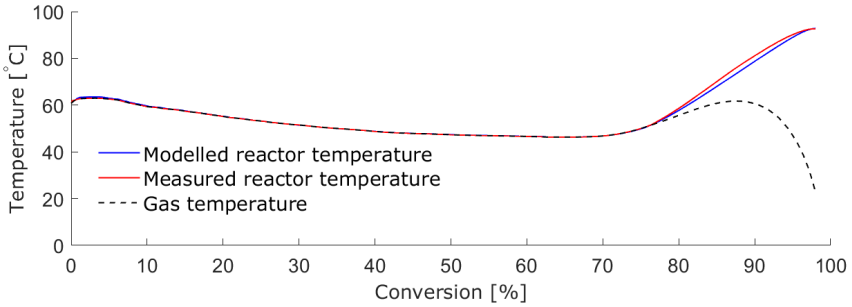

Figure 6.10: Modelled and measured reactor temperature, in addition to the gas temperature. The simulation was run with recursive filtering

The modelled pressure in figure 6.11 follows the same trend as the modelled pressure from the ballistic simulations, but improves the prediction towards the end of the batch. Even though there are no estimated parameters that directly affect the pressure, a significant improvement is observed. The improvement is thought to come from an indirect effect of the estimated parameters and the good prediction of the reactor temperature, which then results in the good pressure prediction. As a result of the good pressure prediction, it is reason to believe that the gas temperature in figure 6.10 is a better reflection of the real gas temperature.

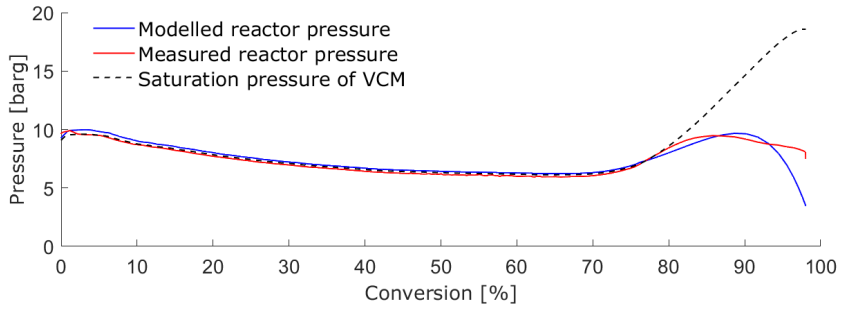

Figure 6.11: Modelled and measured reactor pressure, in addition to the saturation pressure of monomer. The simulation was run with recursive filtering.

Figure 6.12 shows the monomer distribution when simulating the system with recursive filtering. The figure shows that the monomer distribution is approximately the same as for the ballistic simulations. The two distributions are approximately the same because the conversion profiles for the two simulations are similar. This implies that the point where the free monomer phase is fully consumed still coincides well with literature.

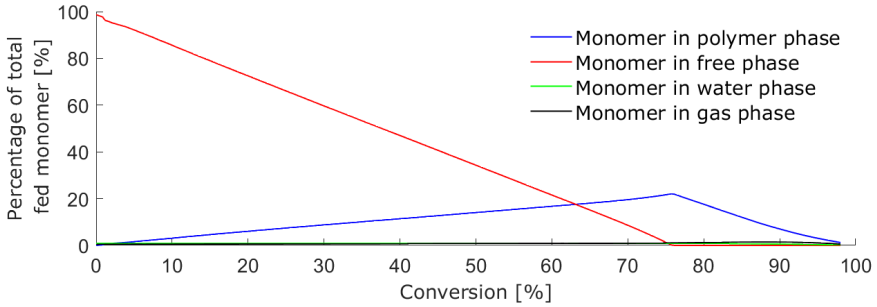

Figure 6.12: The distribution of monomer in all four phases. The simulation was run with recursive filtering.

Figure 6.13 shows the modelled and measured outlet temperature of the cooling jacket, in addition to the measured inlet temperature. Since there was just a small mismatch even without filtering, the improvement is not substantial. However some improvement can be observed, especially towards the end of the batch where the mismatch was the most significant in the ballistic simulations.

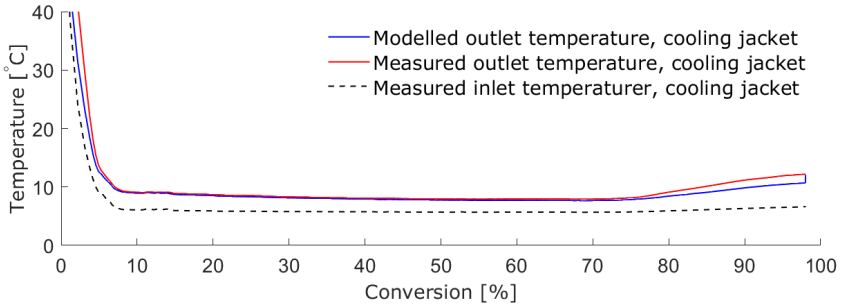

Figure 6.13: Modelled and measured outlet temperature of the cooling jacket, in addition to measured inlet temperature of the cooling jacket. The simulation was run with recursive filtering

The modelled outlet temperature of the reflux condenser in figure 6.14 shows improvement compared to the ballistic simulations in figure 6.7. The modelled temperature with recursive filtering better predicts the more rapid fluctuations in addition to accurately predicting the overall trend. There are still some mismatch at the start of the batch, but this is not substantial. In the same manner as with the ballistic simulations, deviation from the measured temperature is irrelevant after the reflux condenser is shut off.

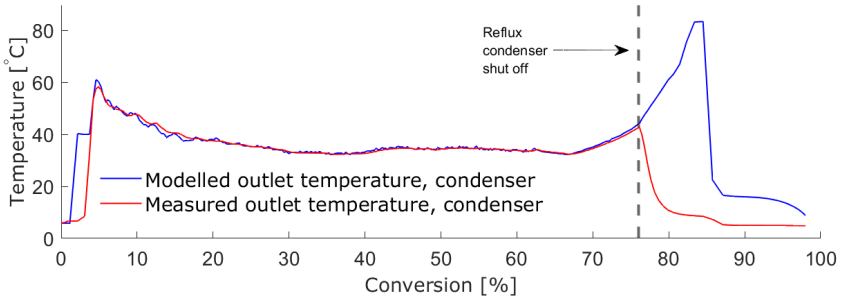

Figure 6.14: Modelled and measured outlet temperature of the reflux condenser. The simulation was run with recursive filtering.

Validation of the Model

Three additional datasets were simulated to validate the model. The results for the different datasets should yield approximately the same results if the model is sufficiently accurate. The results should also adjust for the specifics of each batch, such as disturbances and initiator dosing. Figure 6.15 shows the estimated parameter profiles for the three parameters which was obtained from the simulations with recursive filtering.

The correction factor for the kinetic parameters shows similar trends for all four batches. Some difference is observed, especially at the end of the batch. This can be due to the estimator turning off at different conversions. The estimator switches off when an input signal indicates that the polymerization stage is over, but the model keeps running until the end of the batch. The increase towards the end can be a results of various reasons. One reason can be that the estimator compensates for a too low polymerization rate towards the end of the batch. A too

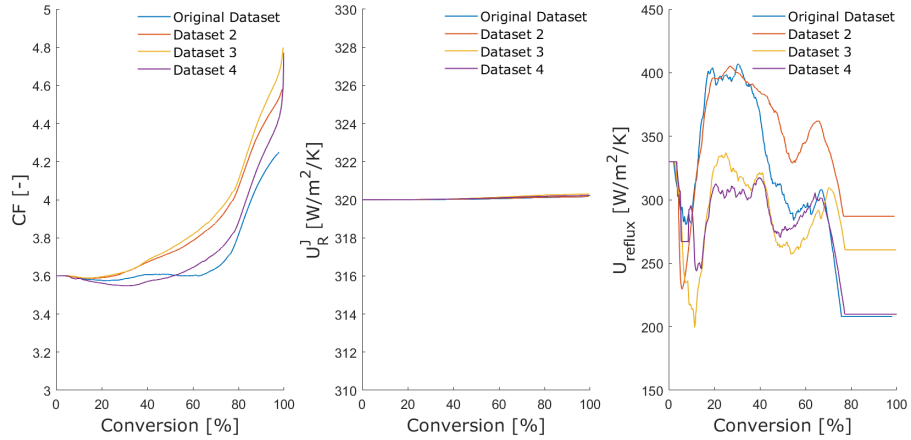

Figure 6.15: Parameter profiles for the correction factor for the kinetic parameters (left), heat transfer coefficient between reactor and cooling jacket (middle) and the heat transfer coefficient for the reflux condenser (right). The parameter profiles were obtained from simulations of the four batches with recursive filtering.

low polymerization rate will result in a too low heat of reaction released. The lack of reaction heat will result in the modelled reactor temperature not achieving the same increase as the measured reactor temperature. Increasing CF will make the reaction rate larges and thus more heat is released to heat up the reactor.

The heat transfer coefficient between the reactor and cooling jacket shows a constant profile for all datasets. Calculations done by INOVYN also suggest that the heat transfer coefficient is approximately constant throughout a single batch. The same constant value for all four datasets also suggests that there are minimal fouling on the reactor walls. A result of the constant profiles is to consider if it is necessary to estimate U_R^J rather than setting the value to be constant.

The profiles for the heat transfer coefficient in the reflux condenser all show the same trends, but they are shifted vertically. This result probably reflects the amount of fouling on the walls of the condenser for the respective dataset. The heat transfer coefficient becomes smaller with an increasing amount of fouling. As the datasets are separated in time, different amounts of fouling will be present depending on the time since last condenser cleaning. The horizontal regions at the end is due to the estimator turning off when the reflux condenser is shut off.

7 Conclusion and Further Work

This report has presented the theoretical aspects of a miniemulsion polymerization process. The theory presented has been used as the foundation in developing a first principal model of a semi-batch reactor for miniemulsion polymerization of VCM. Due to the complex nature of a miniemulsion polymerization, several assumptions were made to be able to model the system. The assumptions were made on the basis that the model should not be too complex and computationally demanding, but still produce sufficiently accurate results.

Uncertain and unknown model parameters were adjusted manually or estimated in Cybernetica's ModelFit environment. A correction factor for the kinetic parameters was introduced because the kinetic parameters from literature was not accurate enough. In addition, kinetic parameters related to the average number of radicals per particle and the mass of initiator in the reactor were unknown. These parameters were altered to produce reasonable profiles for the two outputs. The two outputs cannot be measured, implying that there are uncertainty to the parameters related to these outputs. The correction factor could then account for this uncertainty in addition to other model errors related to the kinetics. Manually adjusting the correction factor gave more accurate results than estimating it using ModelFit. Parameters such as the heat transfer coefficients for the cooling jacket and the reflux condenser were successfully estimated using ModelFit, with only minor manual adjustments. Even though the parameter values listed in table 6.1 gave acceptable results for the ballistic simulations, the model still deviated from the measurements.

The reactor temperature is critical in a polymerization process, so the mismatch between modelled and measured reactor temperature was the main motivation for the implementation of online state- and parameter estimation. This was implemented in the form of the extended Kalman filter. Simulations with the recursive filtering significantly improved the performance of the model. An additional three batches were simulated with recursive filtering, and the results from the model validation showed the same trends with only some variations from batch to batch. The good coherence in the results for all four batches, especially in the correction factor for the kinetic parameters, suggested that the model captured the mechanisms of the process well. Only some minor mismatch was observed for the simulations with recursive filtering, and the results were considered to be satisfactory.

As the work for this project required some limitations due to a limited amount of time available, some aspects should be explored in further detail. The main aspect is to model the estimated parameters in figure 6.15, especially CF, as a function of conversion. This is due to the systematic trend observed in all four batches. Modelling CF as a function of conversion might lead to a better description of the changes in conditions during the batch evolution. In addition, it should be considered if it is necessary to estimate U_R^J online due to the constant parameter profiles obtained for this parameter. Another aspect could be to add more detail to the initiator mechanism. A more detailed description of the initiator system could might capture the dynamics of the complex system in a better way. Modelling the number of particles as a ramp starting from zero and ending up at the final number at some conversion is another aspect to look into. This could improve the performance of the model at the very start of the batch. Finally, a time constant could be introduced to model the slowness of the system. This could might add more detail to the reaction mechanisms such as the initiator system.

The aim of this project was to explore the possibilities of implementing NMPC in the process. A sufficiently accurate model is necessary for the implementation of NMPC. With a good model, NMPC can be a good candidate to improve operation. The results obtained are concluded to be satisfactory, implying that the implementation of NMPC should be explored in further detail.

References

[1] Lars Egil Helseth. *Polyvinylklorid*. http://snl.no/polyvinylklorid. Accessed: 27/11-22. 2022.

[2] W. Harmon Ray and Carlos M. Villa. "Nonlinear dynamics found in polymerization processes — a review". In: *Chemical Engineering Science* 55.2 (2000), pp. 275–290. DOI: https://doi.org/10.1016/S0009-2509(99)00323-1.

[3] C Kiparissides et al. "Dynamic simulation of industrial poly (vinyl chloride) batch suspension polymerization reactors". In: *Industrial & engineering chemistry research* 36.4 (1997), pp. 1253–1267.

[4] Thor Mejdell et al. "Modelling of industrial S-PVC reactor". In: *Chemical engineering science* 54.13-14 (1999), pp. 2459–2466.

[5] Paul C Painter. *Fundamentals of polymer science : an introductory text*. eng. Boca Raton, Fla, 1997.

[6] Lars Egil Helseth. *Homopolymerer*. https://snl.no/homopolymerer. Accessed: 8/10-22. 2019.

[7] Lars Egil Helseth. *Kopolymerer*. https://snl.no/kopolymerer. Accessed: 8/10-22. 2019.

[8] Paul J Flory. "Fundamental principles of condensation polymerization." In: *Chemical Reviews* 39.1 (1946), pp. 137–197.

[9] "Radical Chain Polymerization". In: *Principles of Polymerization*. John Wiley & Sons, Ltd, 2004. Chap. 3, 4, pp. 198–371. ISBN: 9780471478751. DOI: https://doi.org/10.1002/047147875X.ch3.

[10] Jose Asua. *Polymer reaction engineering*. John Wiley & Sons, 2008.

[11] A.S. Sarac. "Redox polymerization". In: *Progress in Polymer Science* 24.8 (1999), pp. 1149–1204. DOI: https://doi.org/10.1016/S0079-6700(99)00026-X.

[12] Krzysztof Matyjaszewski and Thomas P. Davis. *Handbook of radical polymerization*. eng. New York: Wiley-Interscience, 2002. ISBN: 047139274X.

[13] Peter A. Lovell and F. Joseph Schork. "Fundamentals of Emulsion Polymerization". In: *Biomacromolecules* 21.11 (2020), pp. 4396–4441. DOI: 10.1021/acs.biomac.0c00769.

[14] A. Valdebenito and M.V. Encinas. "Thiophenols as chain transfer agents in the polymerization of vinyl monomers". In: *Polymer* 46.24 (2005), pp. 10658–10662. DOI: https://doi.org/10.1016/j.polymer.2005.09.051.

[15] William D Harkins. "A general theory of the reaction loci in emulsion polymerization". In: *The Journal of chemical physics* 13.9 (1945), pp. 381–382.

[16] William D Harkins. "A general theory of the reaction loci in emulsion polymerization. II". In: *The Journal of Chemical Physics* 14.1 (1946), pp. 47–48.

[17] Finn Knut Hansen. "Historic overview". In: *Chemistry and Technology of Emulsion Polymerisation* (2013), pp. 1–22.

[18] J Ugelstad, MS El-Aasser, and JW Vanderhoff. "Emulsion polymerization: Initiation of polymerization in monomer droplets". In: *Journal of Polymer Science: Polymer Letters Edition* 11.8 (1973), pp. 503–513.

[19] José M. Asua. "Miniemulsion polymerization". In: *Progress in Polymer Science* 27.7 (2002), pp. 1283–1346. DOI: https://doi.org/10.1016/S0079-6700(02)00010-2.

[20] CS Chern. "Emulsion polymerization mechanisms and kinetics". In: *Progress in polymer science* 31.5 (2006), pp. 443–486.

[21] F Joseph Schork et al. "Miniemulsion polymerization". In: *Polymer particles* (2005), pp. 129–255.

[22] M. Cioffi, A.C. Hoffmann, and L.P.B.M. Janssen. "Reducing the gel effect in free radical polymerization". In: *Chemical Engineering Science* 56.3 (2001), pp. 911–915. DOI: https://doi.org/10.1016/S0009-2509(00)00305-5.

[23] Wendell V Smith and Roswell H Ewart. "Kinetics of emulsion polymerization". In: *The journal of chemical physics* 16.6 (1948), pp. 592–599.

[24] Stuart C Thickett and Robert G Gilbert. "Emulsion polymerization: State of the art in kinetics and mechanisms". In: *Polymer* 48.24 (2007), pp. 6965–6991.

[25] Bo-Geng Li and Brian W Brooks. "Prediction of the average number of radicals per particle for emulsion polymerization". In: *Journal of Polymer Science Part A: Polymer Chemistry* 31.9 (1993), pp. 2397–2402.

[26] J Ugelstad et al. "A kinetic investigation of the emulsion polymerization of vinyl chloride". In: *Journal of Polymer Science Part C: Polymer Symposia*. Vol. 27. 1. Wiley Online Library. 1969, pp. 49–68.

[27] Mohamed S El-Aasser, E David Sudol, et al. "Miniemulsions: Overview of Research and applications". In: *JCT Res* 1.1 (2004), pp. 21–31.

[28] Stephen Wright, Jorge Nocedal, et al. "Numerical optimization". In: *Springer Science* 35.67-68 (1999), p. 7.

[29] Bjarne Foss and Tor Aksel N. Heirung. *Merging Optimization and Control*. Mar. 2016. ISBN: 978-82-7842-201-4.

[30] Tor Steinar Schei. "On-line estimation for process control and optimization applications". In: *Journal of Process Control* 18.9 (2008), pp. 821–828.

[31] Ahmed H. Abdel-Alim and A. E. Hamielec. "Bulk polymerization of vinyl chloride". In: *Journal of Applied Polymer Science* 16.3 (1972), pp. 783–799. DOI: https://doi.org/10.1002/app.1972.070160321.

[32] H. Scott Fogler. *Elements of chemical reaction engineering*. eng. 4th ed. Boston: Prentice Hall, 2016.

[33] Holger Nilsson, Christer Silvegren, and Bertil Törnell. "Swelling of PVC latex particles by VCM". In: *European Polymer Journal* 14.9 (1978), pp. 737–741.

[34] E Peggion, F Testa, and G Talamini. "A kinetic study on the emulsion polymerization of vinyl chloride". In: *Die Makromolekulare Chemie: Macromolecular Chemistry and Physics* 71.1 (1964), pp. 173–183.

[35] Johannes Brandrup et al. *Polymer handbook*. Vol. 89. Wiley New York, 1999.

A Physical Properties

Expressions and values for the physical properties used in the model equations are listed below. The parameter ϑ is defined as $\vartheta = T - 273.15$ and is the temperature in °C. Physical properties for the components are taken from Kiparissides et al.[3], while the value for the heat of reaction are taken from Brandrup et al.[35].

$$M_W = 18 \cdot 10^{-3} \quad [\text{kg/mol}] \tag{A.1}$$
$$\rho_W^l = 1011.0 - 0.4484\vartheta \quad [\text{kg/m}^3] \tag{A.2}$$
$$C_{p,W} = 4.02 \cdot 10^3 \exp\left(1.99 \cdot 10^{-4} T\right) \quad [\text{J/kg/K}] \tag{A.3}$$
$$p_W^{sat} = \exp\left(72.55 - 7206.7/T - 7.1382 \ln(T) + 4.046 \cdot 10^{-6} T^2\right) \quad [\text{Pa}] \tag{A.4}$$
$$\tag{A.5}$$
$$M_M = 62.5 \cdot 10^{-3} \quad [\text{kg/mol}] \tag{A.6}$$
$$\rho_M^l = 947.1 - 1746\vartheta - 3.24 \cdot 10^{-3}\vartheta^2 \quad [\text{kg/m}^3] \tag{A.7}$$
$$C_{p,M} = 66.848(18.67 + 0.0758\vartheta) \quad [\text{J/kg/K}] \tag{A.8}$$
$$p_M^{sat} = \exp\left(126.85 - 5760.1/T - 17.914 \ln(T) + 2.4917 \cdot 10^{-6} T^2\right) \quad [\text{Pa}] \tag{A.9}$$
$$\tag{A.10}$$
$$\rho_P = 10^3 \exp\left(0.4296 - 3.274 \cdot 10^{-4} T\right) \quad [\text{kg/m}^3] \tag{A.11}$$
$$C_{p,P} = 0.934 \quad [\text{J/kg/K}] \tag{A.12}$$
$$\tag{A.13}$$
$$\Delta H_{rx} = -97.6 \quad [\text{kJ/mol}] \tag{A.14}$$
$$\tag{A.15}$$
$$C_{p,steel} = 502.416 \quad [\text{J/kg/K}] \tag{A.16}$$
$$\tag{A.17}$$
$$R = 8.314 \quad [\text{J/K/mol}] \tag{A.18}$$

In addition to the expressions listed above, the density of gaseous monomer, ρ_M^g, is required for the model. The density of the gaseous monomer is calculated from the virial equation of state. The necessary code is shown below with permission from Peter Singstad, Cybernetica.

```
double rho_vcm_g(   // Out: Dens. for water, kg/m3
  double T,    // In: temperature, K
  double p     // In: Pressure, Pa
)
{
  double rho, Bm, Bw, Bmw;

  fugpar(&Bm, &Bw, &Bmw, T);
  rho = MWm * p / (R_un_gas * T + Bm * p);

  return rho;
}

void fugpar(
  double* Bm,      /* Out: [m3/kmol]    */
  double* Bw,      /* Out: [m3/kmol]    */
  double* Bmw,       /* Out: [m3/kmol]    */
  double T         /* In:  [K]        */
)
{
  double Tc_m = 432.0;       /* [K]             */
  double Tc_w = 647.5;       /* [K]             */
  double Tc_mw = 528.9;      /* [K]             */
  double Pc_m = 56.e5;       /* [Pa]            */
  double Pc_w = 220.5e5;       /* [Pa]            */
  double Pc_mw = 107.e5;       /* [Pa]            */
```

```
  double acfm = 0.1048;      /* [-]             */
  double acfw = 0.3342;      /* [-]             */
  double acfmw = 0.2195;       /* [-]             */
  double Trm, Trw, Trmw;

  Trm = T / Tc_m;
  Trw = T / Tc_w;
  Trmw = T / Tc_mw;

  *Bm = R_un_gas * Tc_m / Pc_m * ((0.083 - 0.422 / pow(Trm, 1.6))
    - acfm * (0.139 - 0.172 / pow(Trm, 4.2)));
  *Bw = R_un_gas * Tc_w / Pc_w * ((0.083 - 0.422 / pow(Trw, 1.6))
    - acfw * (0.139 - 0.172 / pow(Trw, 4.2)));
  *Bmw = R_un_gas * Tc_mw / Pc_mw * ((0.083 - 0.422 / pow(Trmw, 1.6))
    - acfmw * (0.139 - 0.172 / pow(Trmw, 4.2)));
}
```

B Derivation of Energy Balances

The derivation of the energy balance is adapted from Fogler[32].

The unsteady-state energy balance for an open well-mixed system with species both entering and leaving the system can be expressed as

$$\frac{d\hat{E}_{sys}}{dt} = \dot{Q} - \dot{W} + \sum F_i E_i\Big|_{in} - \sum F_i E_i\Big|_{out} \tag{B.1}$$

Here $\dot{Q}$ is the rate of flow of heat to the system, $\dot{W}$ is the rate of work done by the system, $E_i F_i\big|_{in}$ is the rate of energy added to the system by mass flow into the system of specie i and $E_i F_i\big|_{out}$ is the rate of energy leaving the system by mass flow out of the system by specie i. The summation is done over all species in the system. A common convention is to split the work term into *flow work* and *other work*, often called *shaft work*, $\dot{W}_s$.

$$\dot{W} = -\sum F_i p\tilde{V}_i\Big|_{in} + \sum F_i p\tilde{V}_i + \dot{W}_s \tag{B.2}$$

Inserting equation B.2 into equation B.1 and groping inlet- and outlet terms, the result is

$$\frac{d\hat{E}_{sys}}{dt} = \dot{Q} - \dot{W}_s + \sum F_i(E_i + p\tilde{V}_i)\Big|_{in} - \sum F_i(E_i + p\tilde{V}_i)\Big|_{out} \tag{B.3}$$

The energy E_i is the sum of the internal energy (U_i), the kinetic energy (E_K) and the potential energy (E_{pot}). In almost all chemical reactor systems, the kinetic and potential energy are negligible compared to the internal energy. As a result the energy E_i is equal to the internal energy U_i. In addition, we recall the definition of enthalpy (H_i) in equation B.4.

$$H_i = U_i + p\tilde{V}_i \tag{B.4}$$

Inserting equation B.4 and the result $E_i = U_i$ into equation B.3 gives

$$\frac{d\hat{E}_{sys}}{dt} = \dot{Q} - \dot{W}_s + \sum F_i H_i\Big|_{in} - \sum F_i H_i\Big|_{out} \tag{B.5}$$

Further, the energy of the system $\hat{E}_{sys}$ can be expressed as follows when the kinetic and potential energy are neglected:

$$\begin{aligned}
\hat{E}_{sys} &= \sum N_i E_i \\
&= \sum N_i U_i \\
&= \sum N_i (H_i - pV_i) \\
&= \sum N_i H_i - p\sum N_i \tilde{V}_i
\end{aligned} \tag{B.6}$$

Here N_i is the amount of moles of species i. It is worth noting that the last term is the total pressure multiplied by the total volume, i.e. pV. When no spatial variations are present in the system, the pV-term can be neglected. Substituting equation B.6 into equation B.5 gives

$$\frac{d(\sum N_i H_i)}{dt} = \dot{Q} - \dot{W}_s + \sum F_i H_i\Big|_{in} - \sum F_i H_i\Big|_{out} \tag{B.7}$$

The left hand side of equation B.7 can be written as

$$\begin{aligned}\frac{d(\sum N_i H_i)}{dt} &= \sum N_i \frac{dH_i}{dt} + \sum H_i \frac{dN_i}{dt} \\ &= \sum N_i C_{p,i} \frac{dT}{dt} + \sum H_i \frac{dN_i}{dt}\end{aligned} \tag{B.8}$$

The molar balance on specie i can be written as

$$\frac{dN_i}{dt} = -\nu_i R_p + F_{i,0} - F_i, \tag{B.9}$$

where ν_i is the stoichiometric coefficient for specie i. It is assumed that the only reaction contributing to the energy is the propagation reaction. By substituting equation B.9 into equation B.8 gives

$$\frac{d(\sum N_i H_i)}{dt} = \sum N_i C_{p,i} \frac{dT}{dt} + \sum \nu_i H_i (-R_p) + \sum F_{i,0} H_i - \sum F_i H_i \tag{B.10}$$

Substituting equation B.10 into equation B.7, recalling that $\sum \nu_i H_i = \Delta H_{rx}$ and solving for the temperature differential gives

$$\frac{dT}{dt} = \frac{\dot{Q} - \dot{W}_s - \sum F_{i,0}(H_i - H_{i,0}) + (-\Delta H_{rx}) R_p}{\sum N_i C_{p,i}} \tag{B.11}$$

Substituting for H_i and $H_{i,0}$ for the case of no phase change gives

$$\frac{dT}{dt} = \frac{\dot{Q} - \dot{W}_s - \sum F_{i,0} C_{p,i}(T - T_{i,0}) + (-\Delta H_{rx}) R_p}{\sum N_i C_{p,i}} \tag{B.12}$$

Changing the heat capacities from molar basis to mass basis gives the final form of the general energy balance, shown in equation B.13.

$$\frac{dT}{dt} = \frac{\dot{Q} - \dot{W}_s + \sum \hat{m}_{i,0} C_{p,i}(T_{i,0} - T) + (-\Delta H_{rx}) R_p}{\sum m_i C_{p,i}} \tag{B.13}$$

The form of the energy balance in equation B.13 is used as the basis for the more specific energy balances for the reactor temperature, the cooling jacket temperature and the reflux condenser temperature.

Reactor Temperature

Neglecting shaft work and assuming that $\dot{Q}$ can be expressed as

$$\begin{aligned}\dot{Q} &= Q_R^{amb} + Q_R^J + Q_{reflux} \\ &= U_R^{amb} A_R^{amb}(T_{amb} - T_R) + U_R^J A_R^J (T_J - T_R) + \hat{m}_{cw}^{reflux} C_{p,CW}^{reflux}(T_{cw,r}^{in} - T_{cw,r}^{out}),\end{aligned} \tag{B.14}$$

where the first term is heat loss to the environment, the second term is heat transfer between the cooling jacket and reactor, and the last term is the heat exchange in the reflux condenser. If the total heat capacity of the reactor steel is also considered, then the energy balance for the reactor temperature can be written as in equation B.15.

$$\begin{aligned}\frac{dT_R}{dt} &= \frac{Q_R^{amb} + Q_R^J + Q_{reflux} + \sum \hat{m}_i^{feed} C_{p,i}^{feed}(T_i^{feed} - T_R) + (-\Delta H_{rx})R_p}{\sum m_i C_{p,i} + m_{steel} C_{p,steel}} \\ &= \frac{Q_J^{amb} + Q_R^J + Q_{reflux} + Q_{feed} + Q_{rx}}{\sum m_i C_{p,i} + m_{steel} C_{p,steel}}\end{aligned} \tag{B.15}$$

Outlet Temperature Cooling Jacket

In the cooling jacket there are no shaft work or no reaction. It is assumed that $\dot{Q}$ can be written as

$$\begin{aligned}\dot{Q} &= Q_J^{amb} + Q_J^R \\ &= U_J^{amb} A_J^{amb}(T_{amb} - T_J) - U_R^J A_R^J (T_J - T_R),\end{aligned} \tag{B.16}$$

where the first term is the heat loss from the cooling jacket to the environment and the second term is the heat exchange between the cooling jacket and the reactor. In the second term, the fact that $Q_J^R = -Q_R^J$ has been utilized. The temperature T_J is the temperature of the jacket, and it is calculated as the average between the inlet- and outlet stream temperature:

$$T_J = \frac{T_J^{in} + T_J^{out}}{2} \tag{B.17}$$

The rate of change in the outlet temperature of the cooling jacket can then be expressed by equation B.18.

$$\begin{aligned}\frac{dT_J^{out}}{dt} &= \frac{Q_J^{amb} - Q_R^J + \hat{m}_J C_{p,j}(T_J^{in} - T_J^{out})}{m_J C_{p,J}} \\ &= \frac{Q_J^{amb} - Q_R^J + Q_{flow}}{m_J C_{p,J}}\end{aligned} \tag{B.18}$$

Here m_J is the mass of the water inside the cooling jacket and Q_{flow} is the energy change caused by the flow of cooling water.

Outlet Temperature of Reflux Condenser

Similarly to the cooling jacket, no shaft work or reaction is present in the reflux condenser. It is assumed that $\dot{Q}$ can be written as

$$\begin{aligned}\dot{Q} &= Q_{ex} \\ &= U_{reflux} A_{reflux}(T^g - T_{reflux}),\end{aligned} \tag{B.19}$$

where Q_{ex} is the heat exchange between the gas and the cooling water and T^g is the gas temperature. The heat loss to the environment is neglected due to the small interfacial area between the condenser and the environment. The temperature T_{reflux} is calculated as the average between the inlet- and outlet stream temperature:

$$T_{reflux} = \frac{T_{cw,r}^{in} + T_{cw,r}^{out}}{2} \tag{B.20}$$

The rate of change in the outlet temperature of the cooling jacket can then be expressed by equation B.21.

$$\begin{aligned}\frac{dT_{reflux}^{out}}{dt} &= \frac{Q_{ex} + \hat{m}_{cw}^{reflux} C_{p,CW}^{reflux} (T_{cw,r}^{in} - T_{cw,r}^{out})}{m_{reflux} C_{p,reflux}} \\ &= \frac{Q_{ex} + Q_{reflux}}{m_{reflux} C_{p,reflux}}\end{aligned} \tag{B.21}$$

Here m_{reflux} is the mass of the water inside the reflux condenser and Q_{reflux} is the energy change caused by the flow of cooling water. Q_{reflux} is the same expression as in equation B.15.

C Phase Equilibria Calculations and Related Code

The code in this section is presented with permission from Peter Singstad, Cybernetica. Only the most relevant and useful code are presented here. The rest of the model code is not presented as it is confidential or not considered to be relevant.

C.1 Monomer in Polymer Phase

The mass of monomer in the polymer phase can be written as

$$\begin{aligned} m_M^p &= V_M^p \rho_M^l \\ &= V^p(1-\varphi)\rho_M^l, \end{aligned} \tag{C.1}$$

where φ is the volume fraction of polymer phase. The volume of the polymer phase, V^p, can be written as the sum of the volume of polymer and the volume monomer in the polymer phase. This leads to the expression

$$m_M^p = \left(\frac{m_M^p}{\rho_M^l} + \frac{m_P}{\rho_P}\right)(1-\varphi)\rho_M^l, \tag{C.2}$$

which can be solved with respect to m_M^p. This gives equation C.3.

$$m_M^p = \frac{m_P \rho_M^l}{\rho_P}\left(\frac{1-\varphi}{\varphi}\right) \tag{C.3}$$

For modelling purposes a correction factor for the solubility of monomer in polymer is introduced. This results in the final expression for the mass of monomer in polymer shown in equation C.4.

$$m_M^p = K_s\left(\frac{\rho_M^l m_P}{\rho_P}\right)\left(\frac{1-\varphi}{\varphi}\right) \tag{C.4}$$

C.2 Monomer in Gas Phase

The mass of monomer in the gas phase can be written as

$$\begin{aligned} m_M^g &= V_m^g \rho_M^g \\ &= (1-w_l)\rho_M^g V_R, \end{aligned} \tag{C.5}$$

where V_R is the total reactor volume and w_l is the liquid volume fraction given by the expression

$$\begin{aligned} w_l &= \frac{1}{V_R}\left(\frac{m_M - m_M^g}{\rho_M^l} + \frac{m_P}{\rho_P} + \frac{m_W - m_W^g}{\rho_W^l}\right) \\ &= \frac{1}{V_R}\left(\frac{m_M}{\rho_M^l} + \frac{m_P}{\rho_P} + \frac{m_W}{\rho_W^l} - \frac{m_M^g}{\rho_M^g} - \frac{m_W^g}{\rho_W^g}\right) \\ &= \frac{1}{V_R}\left(V_{fluid,s} - \frac{m_M^g}{\rho_M^g} - \frac{m_W^g}{\rho_W^g}\right), \end{aligned} \tag{C.6}$$

where $V_{fluid,s}$ is defined as

$$V_{fluid,s} = \frac{m_M}{\rho_M^l} + \frac{m_P}{\rho_P} + \frac{m_W}{\rho_W^l}, \tag{C.7}$$

and represents the volume of the liquid and solids in the system if neither monomer or water were present in the gas phase. The mass of water in the gas phase is assumed to be negligible compared to the mass of monomer in the gas phase. This leads the expression

$$m_M^g = \left[1 - \frac{1}{V_R}\left(V_{fluid,s} - \frac{m_M^g}{\rho_M^g}\right)\right]\rho_M^g V_R \tag{C.8}$$

Simplifying and rearranging gives the final expression for the mass of monomer in the gas phase shown in equation C.9.

$$m_M^g = (V_R - V_{fluid,s})\frac{\rho_M^l \rho_M^g}{\rho_M^l - \rho_M^g} \tag{C.9}$$

C.3 Monomer Distribution and Phase Equilibria for Interval I and II

The following code performs the phase equilibria calculations for interval I and II. The function inputs and outputs are briefly described at the start of the function. Some comments are added to briefly describe the calculations performed. The calculations performed are presented in section 5.3.

```
int phase_distribution_free(  // Out: Value is 1 if no free phase is found
  double* p,          // Out: Pressure, Pa
  double* Tg,         // Out: Gas temperature, K
  double* mm_p,         // Out: Mass of monomer solved in polymer, kg
  double* mm_w,         // Out: Mass of monomer solved in water, kg
  double* mm_g,         // Out: Mass of monomer in gas phase, kg
  double* mm_f,         // Out: Mass of monomer in free phase, kg
  double* V_l,        // Out: Volume of liquid and solids, m3
  double* cm_p,       // Out: Concentration of monomer in polymer phase, mol/m3
  double* mw_g,       // Out: Mass of water in gas phase, kg
  double* V_p,        // Out: Volume of polymer phase, m3
  double* V_f,        // Out: Volume of free phase, m3
  double* V_g,        // Out: Volume of gas phase, m3
  double* V_w,        // Out: Volume of water phase, m3

  double T,           // In:  Temperature, K
  double mm,          // In:  Monomer mass, kg
  double mw,          // In:  Water mass, kg
  double mp,          // In:  Polymer mass, kg
  double Vr,          // In:  Reactor volume, m3
  double Ks,          // In:  Correction factor for VCM solvability in PVC
  double mm_dos,        // In:  Amount of added monomer, kg
  double Xm         // In:  Conversion of monomer
)
{
  double rhoW, rhoP, rhoM, rhoG, vf, am, pM, pW, V_fluid_s, z, yM, yW;

  psat(&pM, &pW, T);      // Get saturation pressures at given reactor temperature
  *p = pM + pW;
  *Tg = T;
  am = 1.0;

  // Calculate densities at given reactor temperature
  rhoW = rho_w(T);
  rhoP = rho_pvc(T);
  rhoM = rho_vcm(T);
  rhoG = rho_vcm_g(*Tg, pM);

  FloryPVC(&vf, am, T);   // Calculation of the volume fraction

  // Molar fractions in gas phase
  yW = pW / *p;
  yM = 1 - yW;
```

```
    // Monomer distribution
    V_fluid_s = mw / rhoW + mp / rhoP + mm / rhoM;
  *mm_g = (Vr - V_fluid_s) * rhoM * rhoG / (rhoM - rhoG);
  *mm_p = (rhoM * Ks * mp * (1 - vf)) / (rhoP * vf);
  *mm_w = 0.0088 * am * mw;
  *mm_f = mm - *mm_g - *mm_w - *mm_p;

  // Volume of phases and total liquid volume (volume in reactor which is not gas)
  *V_g = * mm_g / (yM * rhoG);
  *V_l = Vr - *V_g;
  *V_p = (Xm * MWm * mm_dos) / rhoP + *mm_p / rhoM;
  *V_f = *mm_f / rhoM;
  *V_w = *V_l - *V_p - *V_f;

  // Concentration of monomer in polymer phase
  *cm_p = *mm_p / (MWm * *V_p);

  //Mass of water in gas phase
  *mw_g = (MWw * yW * *V_g * *p) / (R_un_gas * *Tg);

  if (*mm_f < 0) {
    *mm_f = 0.0;  // There is no free VCM
    return 1;
  }
  return 0;
}
```

C.4 Calculation of Volume Fraction of Polymer in the Polymer Phase for Interval I and II

The following code computes the volume fraction of polymer in the polymer phase for interval I and II. The calculation appears in the code in appendix C.3. This calculation also includes the calculation of the interaction parameter.

```
void FloryPVC(
  double* vf,   // Out: volume fraction of solid material
  double am,    // In: activity coefficient
  double T      // In: temperature [K]
)
{
  double x, r, dr, c0, c1, c2, c3, c4;
  long i;

  // Check for singularity - in case of no monomer present
  if (am < 1.0e-15) {
    *vf = 1.0;
    return;
  }
  else if (am > 1.0) {
    am = 1.0;
  }

  // Parameters for Flory-Huggin's relation adapted for PVC
  CoeffFlory(&c4, &c3, &c2, &c1, &c0, T, am);

  // Initial guess
  x = 1.0 - 0.25 * am * am * am * (1.0 + (T - 323.15) / 500);

  // Newton-Raphson iteration to find volume fraction
  for (i = 0; i < 3; i++) {
    r = log(1 - x) + (((c4 * x + c3) * x + c2) * x + c1) * x + c0;
    dr = 1 / (x - 1) + ((4 * c4 * x + 3 * c3) * x + 2 * c2) * x + c1;

    x = x - r / dr;
  }
```

```
  *vf = x;
}
```

C.5 Monomer Distribution and Phase Equilibria for Interval III

The following code performs the phase equilibria calculations for interval III. The function inputs and outputs are briefly described at the start of the function. Some comments are added to briefly describe the calculations performed. The calculations performed are presented in section 5.3.

```
void phase_distribution_unfree(
  double* p,         // Out: Pressure, Pa
  double* Tg,        // Out: Gas temperature, K
  double* mm_p,        // Out: Mass of monomer solved in polymer, kg
  double* mm_w,        // Out: Mass of monomer solved in water, kg
  double* mm_g,        // Out: Mass of monomer in gas phase, kg
  double* mw_g,      // Out: Mass of water in gas phase, kg
  double* cm_p,      // Out: Concentration of monomer in polymer phase, mol/m3
  double* V_l,       // Out: Volume of liquid and solids, m3
  double* V_g,       // Out: Volume of gas phase, m3
  double* V_p,       // Out: Volume of polymer phase, m3
  double* V_w,       // Out: Volume of water phase, m3

  double T,          // In:  Temperature, K
  double mm,         // In:  Monomer mass, kg
  double mw,         // In:  Water mass, kg
  double mp,         // In:  Polymer mass, kg
  double Vr,         // In:  Reactor volume, m3
  double Ks,         // In:  Correction factor for VCM solvability in PVC
  double mm_dos,       // In:  Amount of added monomer
  double Xm       // In:  Conversion of monomer
)
{
  // This function assumes no free VCM present in the system
  double rhoW, rhoP, rhoM, rhoG, mm_p_iter, vf, am, pM, pW, V_fluid_s, yM, yW, z;
  int i;

  // Parameters in the numerical solution
  double zeta = 0.5;
  int N = 3;

    // Calculation of densities at give nreactor temperature
  rhoW = rho_w(T);
  rhoP = rho_pvc(T);
  rhoM = rho_vcm(T);

  mm_p_iter = mm; // First assume that all VCM is in the polymer phase. ''Initial
      guess''

  for (i = 1; i <= N; i++) {
    vf = (rhoM * Ks * mp) / (rhoM * Ks * mp + rhoP * mm_p_iter);   // Calculation of
        volume fraction
    InvFloryPVC(&am, T, vf);  // Activity from inversely solving Flory-Huggins eq
    psat(&pM, &pW, T);  // Saturation pressures at given reactor temperature

    if (am > 1) {
      am = 1.0;
    }
    *p = pM * am + pW;
    *Tg = Tsat_vcm(pM * am); // Gas temperature at given partial pressure of VCM
    rhoG = rho_vcm_g(*Tg, pM * am);
    // Monomer distribution
    V_fluid_s = mw / rhoW + mp / rhoP + mm / rhoM;
    *mm_g = (Vr - V_fluid_s) * rhoM * rhoG / (rhoM - rhoG);
    *mm_w = 0.0088 * am * mw;
    *mm_p = mm - *mm_g - *mm_w;
     // Update value of mass of monomer in polymer phase
```

```
    mm_p_iter = zeta * *mm_p + (1 - zeta) * mm_p_iter;
  }

  // Molar fraction in gas
  yM = 1 - pW / (*p);
  yW = pW / (*p);

  // Volume of phases and total liquid volume (volume in reactor which is not gas)
  *V_g = * mm_g / (yM * rhoG);
  *V_p = *mm_p / rhoM + (mm_dos * Xm * MWm) / rhoP;
  *V_l = Vr - *V_g;
  *V_w = *V_l - *V_p;

  // Concentration of monomer in polymer phase
  *cm_p = * mm_p / (MWm * *V_p);

  // Mass of water in gas phase
  *mw_g = (yW * *p * *V_g * MWw) / (R_un_gas * *Tg);
}
```

C.6 Calculation of Monomer Activity for Interval III

The following code computes the activity of the monomer in interval III. The calculation is a part of the calculation routine outlined in algorithm 1 and also appears in the code in appendix C.5. This calculation also includes the calculation of the interaction parameter.

```
void InvFloryPVC(
  double* am,       // Out: activity coefficient
  double T,     // In: temperature [K]
  double vf     // In: volume fraction of solid material
)
{
  double c0, c1, c2, c3, c4;

  // Parameters for Flory-Huggin's relation adapted for PVC
  CoeffFlory(&c4, &c3, &c2, &c1, &c0, T, 1.0);

  if (vf >= 1.0) {
    *am = 0.0;
    return;
  }
  else if (vf <= 0.0) {
    *am = 1.0;
    return;
  }

  // Inverse solution of the Flory-Huggins equation. The c-coefficients are part of
     the calculation of the interaction parameter
  c0 = log(1 - vf) + (((c4 * vf + c3) * vf + c2) * vf + c1) * vf;
  *am = exp(c0);
}
```

C.7 Flory-Huggins Coefficients

The following code calculates the parameters used in the Flory-Huggins equation. The parameters are used in the calculation of the Flory-Huggins interaction parameter.

```
void CoeffFlory(
  double* c4,   // Out: Parameter
  double* c3,   // Out: Parameter
  double* c2,   // Out: Parameter
  double* c1,   // Out: Parameter
  double* c0,   // Out: Parameter
  double T,     // In: temperature [K]
  double am     // In: activity coefficient
```

```
)
{
  double FH_Xs  = 0.26;          // [ - ]
  double FH_a = 0.15524;         // [ - ]
  double FH_b = 0.35311;         // [ - ]
  double FH_c = -0.50527;        // [ - ]
  double FH_d = 11.3605;         // [K]
  double FH_e = 199.96;        // [K]
  double FH_f = 6244.49;         // [K]

  double cT;

  cT = FH_f / T;

    // Parameters for the Flory-Huggins equation adapted to PVC
  *c4 = cT * FH_b;
  *c3 = cT * FH_c;
  *c2 = (FH_e + FH_f * FH_a + cT * FH_d) / T + FH_Xs;
  *c1 = 1.0;
  *c0 = -log(am);
}
```

C.8 Gas Temperature in Interval III

The following code calculates the gas temperature in interval III. The gas temperature is calculated from the partial pressure of the monomer.

```
double Tsat_vcm(
  double p      /* In: Pressure [Pa]  */
)
{
  double T, pvcm, pw;

  double a = 5e5 / 20;
  int i;
  T = (p - 1e6) / a + 60 + 273.15;
  for (i = 0; i < 5; i++) {
    psat(&pvcm, &pw, T);
    T = (p - pvcm) / a + T;
  }
  return T;
}
```

D Miscellaneous plots

D.1 Reactor Temperature as a Function of Time

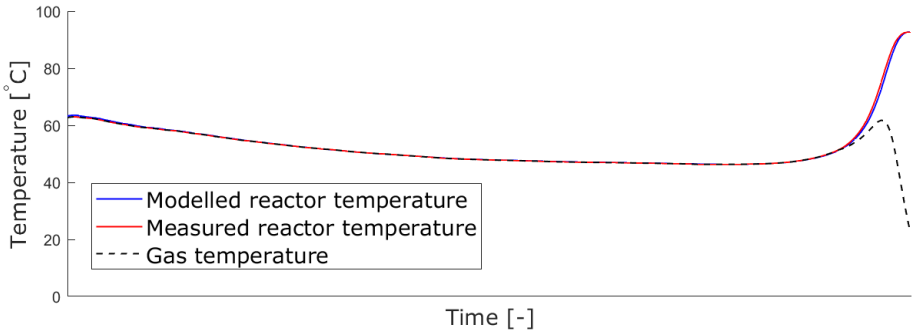

Figure D.1: Reactor temperature plotted as a function of time. The purpose of the plot is to better show the steep temperature increase. The time axis is unitless in order to mask the time.